Received: 11 October 2017 | Revised: 28 June 2018 | Accepted: 31 August 2018

DOI: 10.1002/rnc.4362

RESEARCH ARTICLE

WILEY

Robust output-feedback control of 3D directional drilling systems

O.A. Villarreal Magaña[1] | F.H.A. Monsieurs[2] | E. Detournay[4] | N. van de Wouw[2,3,4]

[1]Dynamic Legged Systems, Istituto Italiano di Tecnologia, Genoa, Italy

[2]Department of Mechanical Engineering, Eindhoven University of Technology, Eindhoven, The Netherlands

[3]Delft Center for Systems and Control, Delft University of Technology, Delft, The Netherlands

[4]Department of Civil, Environmental, and Geo-Engineering, University of Minnesota, Minneapolis, Minnesota

Correspondence
O.A. Villarreal Magaña, Istituto Italiano di Tecnologia, Via Morego, 30, 16163 Genoa, Italy.
Email: octavio.villarreal@iit.it

Present Address
O.A. Villarreal Magaña, via Morego, 30, 16163 Genoa, Italy.

Summary

This paper introduces a robust observer-based output feedback control strategy that enables the generation of complex three-dimensional borehole trajectories created by directional drilling systems, while avoiding undesired transient behavior. The model-based controller relies on a set of nonlinear delay differential equations describing the borehole evolution. Herein, only local orientation measurements of the bottom hole assembly of the drilling system are employed. Controller and observer gains are synthesized by optimizing the location of the rightmost pole of the closed-loop dynamics, using a spectral approach for delay differential equations. Moreover, the strategy is extended to cope with the uncertainty of key system parameters in the directional drilling process. The effectiveness of the designed controller is tested in an illustrative benchmark study.

KEYWORDS

delay differential equations, directional drilling, nonlinear systems, output-feedback, robust control, tracking control

1 | INTRODUCTION

In the past few decades, the exhaustion of oil, mineral, and gas has been a topic of great concern to the scientific and engineering community. In this regard, one of the recent goals of the industry is enabling the extraction of resources located in difficult-to-reach reservoirs. One of the new technologies that has been developed in order to access such resources is directional drilling, which makes it possible to drill boreholes with complex trajectories using a downhole robotic actuator called a rotary steerable system (RSS).[1,2] The purpose of this research is to propose a novel control strategy supporting the accurate and robust generation of three-dimensional (3D) boreholes using such an RSS actuation system.

Despite the fact that directional drilling has enabled the possibility of accessing hard-to-reach reservoirs, several challenges remain in practice. The directional drilling process is nowadays still governed by experienced human drillers, which are in charge of manipulating the RSS actuator to control the orientation of the bit and, therefore, the borehole evolution. Experimental evidence has shown that state-of-practice directional drilling techniques can induce borehole oscillations.[3,4] These oscillations in the borehole geometry are undesirable as they (i) compromise borehole stability, (ii) reduce drilling efficiency, (iii) make it more difficult to insert the borehole casing in preparation for production, and (iv) reduce the rate of penetration (ie, the speed of the drilling process). In this work, we aim to develop a model-based

This work was performed while the first author was affiliated with the Delft Center for Systems and Control, Faculty of Mechanical, Maritime and Materials Engineering, Delft University of Technology, The Netherlands.

controller synthesis approach, which enables the drilling of complex 3D borehole geometries while preventing borehole spiraling, using only measurements available in practice.

Several works exist on the topic of the control of directional drilling processes. Some works on input-output correlation models have been proposed in the work of Matheus et al[5]; herein, no clear explanation on the evolution of the system dynamics regarding the influence of forces in the model or the controller itself is given. In the works of Panchal et al,[6-8] controllers are developed based on empirical models of the borehole propagation process, in which a direct link between the force applied by the RSS and the curvature of the borehole is assumed. This approach ignores the (physically relevant) transient behavior of the borehole propagation, which is essential in preventing borehole spiraling. In the work of Bayliss and Matheus,[9] a state-space model for borehole propagation is derived, and on the basis of this model, a controller is designed. However, the essential delay nature of the borehole propagation dynamics[10-12] is not captured in this model. In the work of Downton and Ignova,[13] a proportional controller to test the closed-loop stability of the directional drilling model developed in the work of Downton[11] was designed, and in the work of Sun et al,[14] using the same model, an $\mathcal{L}_1$ adaptive controller was designed. In the works of Kremers et al[15] and van de Wouw et al,[16] a robust *output-feedback* approach for inclination control was proposed based on the model in the work of Perneder.[12]

All of the aforementioned works rely on the full availability of the measurements of the orientation of the borehole at the bit (ie, full state information), which, in practice, is not possible. Some exceptions are the works of Kremers et al[15] and van de Wouw et al,[16] in which a robust output-feedback control strategy was proposed. Furthermore, a majority of the considered control approaches focus on *two-dimensional* directional drilling models. However, in practice, complex *3D* borehole geometries need to be generated. An exception is the recent preliminary work of van de Wouw et al,[17] in which a state-feedback control strategy for 3D directional drilling processes was proposed on the basis of the 3D model in the work of Perneder.[12]

Now, the main challenge taken on in this paper is the development of a control strategy for *3D directional drilling processes* that (i) prevents the occurrence of borehole oscillations, (ii) only employs practically available sensor measurements of the orientation of the bottom hole assembly (BHA), and (iii) ensures robustness against key uncertainties, such as those in the weight on bit and bit walk. In this scope, we care to stress that the dynamics of 3D directional drilling processes are significantly more complex than their two-dimensional counterpart due to, first, the presence of nonlinearities and, second, the multivariable nature of the process.

The main contribution of this work is the development of a controller design strategy for 3D drilling systems, which relies only on local measurements of the orientation of the BHA. The proposed control strategy is based on the borehole propagation model in the work of Perneder,[12] which has been shown able to capture the key dynamics of the process.[4]

We extend the state-feedback control strategy proposed in the work of van de Wouw et al,[17] by designing an observer that estimates the orientation variables, instead of considering these states to be directly measurable. In practice, directional drilling systems only have access to the measurements of the orientation of the BHA, which is different from the orientation of the borehole. This is why we perform the estimation of the borehole orientation only using measurements that are available in a realistic drilling scenario. Moreover, in the work of van de Wouw et al,[17] an input transformation is used to decouple the two key borehole orientation dynamics, ie, the inclination and azimuth dynamics, into two identical systems, which simplifies controller design. Due to the differences between the estimated and actual orientation variables, such a decoupling approach is not possible. In this paper, the stability of the resulting coupled (error) dynamics is analyzed using cascaded system properties and an optimization-based spectral controller and observer tuning approach. An additional contribution is the fact that the robustness of the proposed output-feedback control strategy for the uncertainty in key system parameters is analyzed and an "a priori" robustly stabilizing controller design strategy is proposed.

The outline of this paper is as follows. In Section 2, the model of a 3D directional drilling system, which is used for controller synthesis, is described. In Section 3, the generation of 3D complex borehole trajectories is formulated as a reference tracking problem. Sections 4 and 5 focus on the controller design for the nominal and robust scenarios, respectively, and a systematic tuning method is proposed for both cases. The performance of the controllers is evaluated via a simulation study of realistic benchmark scenarios in Section 6. The conclusion of this work is given in Section 7.

2 | MODEL OF A 3D DIRECTIONAL DRILLING SYSTEM

The model used as a basis for controller synthesis is described in the works of Perneder[12] and Perneder and Detournay.[18-20] Figure 1 shows the geometric description of the 3D directional drilling system.

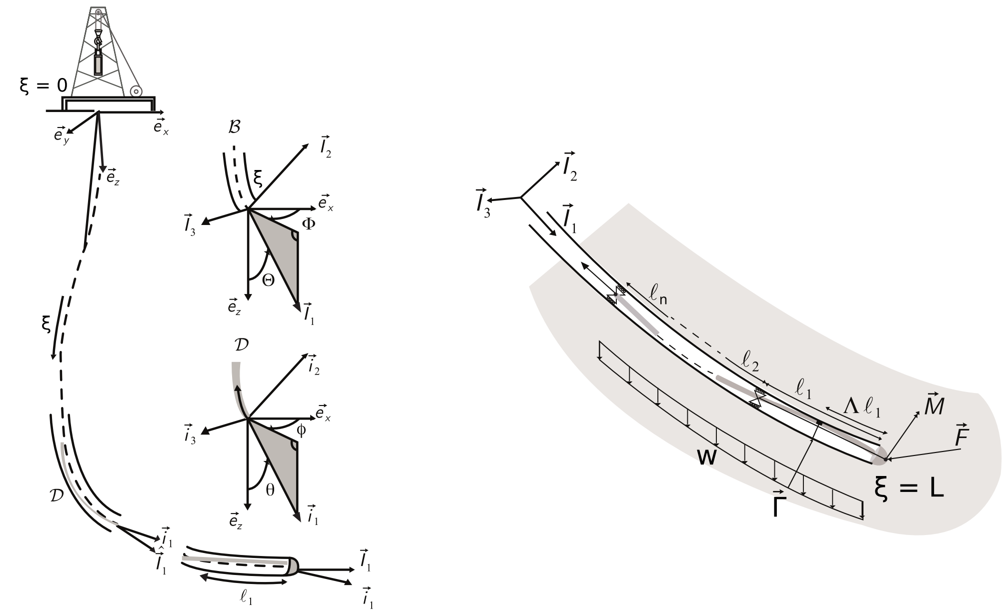

FIGURE 1 Geometric description of a directional drilling system (left) as well as the borehole axis and the bottom hole assembly (BHA) axis (right). Deflected BHA [Colour figure can be viewed at wileyonlinelibrary.com]

The predominant element that affects the borehole evolution is the so-called BHA, which is the lowest part of the drill string and is usually equipped with three to five stabilizers in order to center it in the borehole, preventing buckling and minimizing lateral vibrations. The model considers the effects of the upper part of the drill string as a mere boundary condition in terms of the axial force transmitted from the drill string to the BHA. The elements of the geometric description of the model are listed below.

1. The earth-fixed coordinate basis is given by $(\vec{e}_x, \vec{e}_y, \vec{e}_z)$. It is located at the drilling rig and vector $\vec{e}_z$ points in the direction of gravity and is perpendicular to $\vec{e}_x$ and $\vec{e}_y$ for a right-handed system.
2. The borehole is described as a function of the curvilinear coordinate ξ, with $0 \leq \xi \leq L$ where 0 is the value of the coordinate at the surface and L is the total length of the borehole.
3. The borehole axis $\mathcal{B}$ is defined as the trajectory of a reference point at the bit.
4. The basis associated with the borehole axis $\mathcal{B}$ $(\vec{I}_1, \vec{I}_2, \vec{I}_3)$ is defined such that $\vec{I}_1$ is the tangent unit vector to $\mathcal{B}$ and $\vec{I}_3 \cdot \vec{e}_y = 0$ (parallel) and $\vec{I}_1 \times \vec{i}_2 = \vec{I}_3$ (perpendicular) and defining the system as right-handed.
5. The borehole inclination Θ is the angle between vector $\vec{e}_z$ and $\vec{I}_1$ as a function of the curvilinear coordinate S.
6. The borehole azimuth Φ is the angle between $\vec{e}_x$ and the projection of $\vec{I}_1$ to the plane spanned by $\vec{e}_x$ and $\vec{e}_y$.
7. The BHA axis $\mathcal{D}$ is considered to be slightly deviated from the borehole axis $\mathcal{B}$ (due to the deflection of the BHA with respect to the borehole axis).
8. The basis associated to the BHA $(\vec{i}_1, \vec{i}_2, \vec{i}_3)$ is defined such that $\vec{i}_1$ is the tangent unit vector to $\mathcal{D}$ and $\vec{i}_3 \cdot \vec{e}_y = 0$ (parallel) and $\vec{i}_1 \times \vec{i}_2 = \vec{i}_3$ (perpendicular) and defining the system as right-handed.
9. It is important to note that, in general, the borehole and BHA axes are not coaxial; thus, in general, $\vec{I}_1 \neq \vec{i}_1$.
10. The BHA inclination θ is the angle between $\vec{e}_z$ and $\vec{i}_1$ as a function of the curvilinear coordinate s.
11. The BHA azimuth ϕ is the angle between $\vec{e}_x$ and the projection of $\vec{i}_1$ to the plane spanned by $\vec{e}_x$ and $\vec{e}_y$.

The mathematical model description is comprised of three main elements: (i) the BHA model, which describes the deflection of the BHA (see Figure 1) and considers the fact that the BHA is constrained by the stabilizers to fit in a borehole that has already been drilled in the past (thereby leading to spatial delays in the model), (ii) the kinematic relationships that relate the motion of the bit to the shape of the generated borehole, and (iii) the bit/rock interface law that represents the interaction between the penetration variables at the bit and the forces and moments acting on the bit ($\hat{\vec{F}}$ and $\hat{\vec{M}}$ in Figure 1), depending on the properties of the bit and the rock that is being drilled. Figure 2 shows the three elements of the model and how these interact.

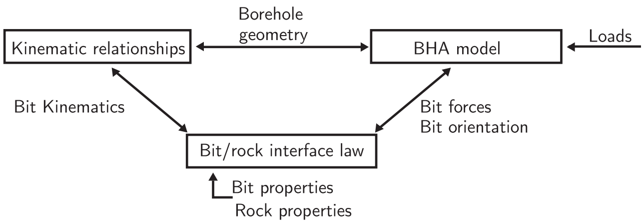

FIGURE 2 Interaction between the elements of the model. BHA, bottom hole assembly

2.1 | Borehole evolution equations

The borehole evolution is governed by a set of nonlinear delay differential equations that describe the inclination Θ and azimuth Φ of the borehole at the bit in terms of the independent variable, being the (dimensionless) length of the borehole $\xi = \frac{L}{\ell_1}$, where L is the total length of the borehole and ℓ_1 is the length between the bit and the first stabilizer (see Figure 1). The model equations are obtained in the work of Perneder[12] and given as follows:

$$\eta\Pi\left((\theta-\Theta)\cos\varpi + \sin\Theta\sin\varpi(\phi-\Phi)\right) = \mathcal{F}_b\left(\theta - \langle\Theta\rangle_1\right) + \mathcal{F}_w\Upsilon\sin\langle\Theta\rangle_1 + \mathcal{F}_r\Gamma_\Theta + \sum_{i=1}^{n-1}\mathcal{F}_i\left(\langle\Theta\rangle_i - \langle\Theta\rangle_{i+1}\right), \tag{1a}$$

$$-\chi\Pi\theta' = \mathcal{M}_b\left(\theta - \langle\Theta\rangle_1\right) + \mathcal{M}_w\Upsilon\sin\langle\Theta\rangle_1 + \mathcal{M}_r\Gamma_\Theta + \sum_{i=1}^{n-1}\mathcal{M}_i\left(\langle\Theta\rangle_i - \langle\Theta\rangle_{i+1}\right), \tag{1b}$$

$$\eta\Pi\left(-(\theta-\Theta)\sin\varpi + \cos\varpi\sin\Theta(\phi-\Phi)\right) = \mathcal{F}_b\left(\phi - \langle\Phi\rangle_1\right)\sin\langle\Theta\rangle_1 + \mathcal{F}_r\Gamma_\Phi + \sum_{i=1}^{n-1}\mathcal{F}_i\left(\langle\Phi\rangle_i - \langle\Phi\rangle_{i+1}\right)\sin\langle\Theta\rangle_1, \tag{1c}$$

$$-\chi\Pi\phi'\sin\theta = \mathcal{M}_b\left(\phi - \langle\Phi\rangle_1\right)\sin\langle\Theta\rangle_1 + \mathcal{M}_r\Gamma_\Phi + \sum_{i=1}^{n-1}\mathcal{M}_i\left(\langle\Phi\rangle_i - \langle\Phi\rangle_{i+1}\right)\sin\langle\Theta\rangle_1. \tag{1d}$$

In (1), the derivatives of the inclination θ and the azimuth ϕ of the BHA at the bit with respect to the dimensionless length (ie, $\frac{d\theta}{d\xi}$ and $\frac{d\phi}{d\xi}$) are given by θ' and ϕ', respectively. The terms $\langle\Theta\rangle_i$ and $\langle\Phi\rangle_i$ (with i indicating the ith section of the BHA in between stabilizers starting from $i = 0$ at the bit; see Figure 1) are the average inclination and azimuth of the borehole between stabilizers, respectively, and are defined as

$$\langle\Theta\rangle_i := \frac{1}{\varkappa_i}\int_{\xi_i}^{\xi_{i-1}}\Theta(\sigma)d\sigma, \qquad \langle\Phi\rangle_i := \frac{1}{\varkappa_i}\int_{\xi_i}^{\xi_{i-1}}\Phi(\sigma)d\sigma. \tag{2}$$

Herein, $\varkappa_i = \frac{\ell_i}{\ell_1}$ (with ℓ_i being the distance between stabilizers $i-1$ and i starting from the bit) denotes the dimensionless length of BHA section i and ξ_i is the dimensionless position of stabilizer i given by $\xi_i(\xi) = \xi - \sum_{j=1}^{i}\varkappa_j$, for $i = 1, 2, \dots, n$, with n being the total number of stabilizers. The terms in (2) introduce distributed delays into the model in (1).

In (1), the parameters denoted by the calligraphic letters $\mathcal{M}$ and $\mathcal{F}$ (with appropriate subindices) are coefficients related to the configuration of the BHA (see the works of Perneder,[12] Monsieurs,[21] and Villarreal Magaña[22]). Two parameters of the system are considered as known, ie, the angular steering resistance η and the lateral steering resistance χ. These parameters represent the resistance to impose lateral and angular penetrations to the bit relative to the axial penetration, respectively.

On the other hand, there are two key parameters in the system that are subject to uncertainty. The first one is denoted by $\Pi = \frac{W_{\text{act}}}{F^*}$, and it defines the dimensionless active weight on bit, with W_{act} being the active weight on bit (axial force on the bit used for cutting) and $F^* = \frac{3E_yI}{\ell_1}$, where E_yI denotes the bending stiffness of the BHA. The parameter Π can be considered as constant (yet uncertain). The source of the uncertainty of Π is related to different factors: changes in the applied hook load at the rig surface and in the drag forces due to the interaction of the borehole with the drill string, decrease in bit sharpness due to wear, and variation in rock properties. The second key parameter is the so-called bit walk angle ϖ, and it quantifies the natural tendency of the bit to drift in a lateral direction while drilling. This parameter is present in the process due to its 3D nature, and it is considered uncertain, since it is affected by the orientation of the bit (which is generally not known) and by the so-called borehole over-gauging (see the work of Chen et al[23]). It has been shown in the works of Marck et al,[4] van de Wouw et al,[17] and Perneder and Detournay[18] that these two parameters are key

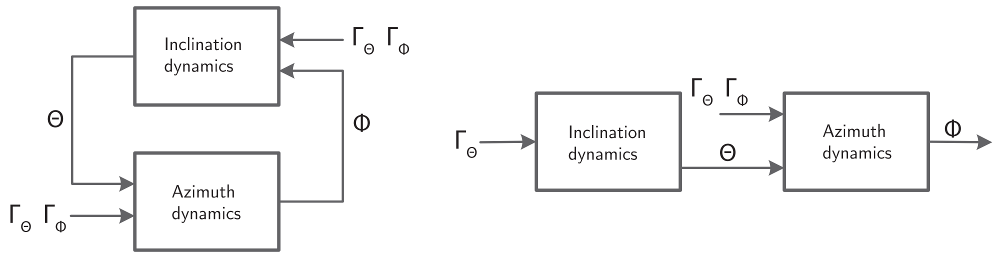

FIGURE 3 Interaction of the Θ-dynamics and Φ-dynamics for non-neutral (left) and neutral (right) bit walk models

to the stability of the borehole evolution and that they are closely related to the borehole spiraling phenomenon, which we aim to avoid by control in this paper.

The external forces acting on the system are the RSS actuator forces and the distributed weight of the BHA (see Figure 1). $\Gamma_i = \frac{F_{\mathrm{rss},i}}{F^*}$, for $i = \Theta, \Phi$, are the scaled RSS forces constituting the control inputs to the system. The RSS force vector $\vec{F}_{\mathrm{rss}}$ is comprised of its perpendicular components $F_{\mathrm{rss},\Theta}$ and $F_{\mathrm{rss},\Phi}$ along the $\vec{I}_2$ and $\vec{I}_3$ axes, respectively (see Figure 1). In Equation (1), specifically in the term $\mathcal{F}_w \Upsilon \sin \langle\Theta\rangle_1$, the scaled distributed weight of the BHA is denoted by Υ, and its influence is considered as a slowly varying disturbance to the system.

Equation (1) shows that the model is composed of four nonlinear (differential) equations with distributed delays. The ultimate goal of the model is to describe the evolution of the borehole orientation (Θ and Φ) and not that of the BHA (θ and ϕ); this means that it would be more convenient to express the BHA orientation variables in terms of the borehole variables, to arrive at a model of the form

$$\begin{aligned} \Theta'(\xi) &= f_\Theta\left(\Theta(\xi), \Phi(\xi), \Gamma_\Theta, \Gamma_\Phi, \Gamma_\Theta{}', \Gamma_\Phi{}'\right), \\ \Phi'(\xi) &= f_\Phi\left(\Theta(\xi), \Phi(\xi), \Gamma_\Theta, \Gamma_\Phi, \Gamma_\Theta{}', \Gamma_\Phi{}'\right), \end{aligned} \tag{3}$$

by eliminating the variables θ and ϕ from (1). In (3), the following notational convention (see the work of Michiels and Niculescu[24]) is used:

$$\Theta_\xi(\sigma) := \Theta(\xi + \sigma), \quad \Phi_\xi(\sigma) := \Phi(\xi + \sigma), \quad \forall \sigma \in [\varkappa_{\mathrm{tot}}, 0],$$

with $\varkappa_{\mathrm{tot}} = \sum_{i=1}^n \varkappa_i$. This can be achieved by solving Equations (1a) and (1c) for θ and ϕ, respectively. The complete expressions of Equation (3) are rather complex; for the sake of brevity, we refer to the works of Monsieurs[21] and Villarreal Magaña[22] for more details. We care to stress though that the delay differential equations in (3) (for the inclination Θ and the azimuth Φ) are mutually coupled (in a nonlinear fashion); this fact is schematically depicted in the scheme on the left of Figure 3. [21] Furthermore, both delay differential equations are also affected by both the RSS actuator forces Γ_Θ and Γ_Φ, and their derivatives. The complexity of the model in (3) (see the work of van de Wouw et al[17]) obstructs controller design, which motivates the use of the model in the absence of the bit walk effect (ie, $\varpi = 0°$ in (1) or (3)) as a basis for controller design. The dynamics of the so-called neutral bit walk model[17] (not to be confused with the neutral-type delay differential equations) are far less complex than the full model described by Equation (1). Due to the absence of the bit walk effect, there is only unilateral coupling from the inclination dynamics to the azimuth dynamics (see Figure 3). In the following section, we introduce the neutral bit walk model as a basis for controller design. In Section 6, we perform a simulation case study validating the proposed control strategy considering the full model equations described by (1).

2.2 | Modeling for control

In order to facilitate controller design, a state-space representation of the dynamical model of the borehole evolution is introduced. Without loss of generality, it can be assumed that a two-stabilizer system captures the key dynamics of the process (see the work of Marck et al[4]). Then, for this two-stabilizer case, the states of the system can be defined as

$$x_\Theta = \begin{bmatrix} \Theta \\ \langle\Theta\rangle_1 \\ \langle\Theta\rangle_2 \end{bmatrix}, \qquad x_\Phi = \begin{bmatrix} \Phi \\ \langle\Phi\rangle_1 \\ \langle\Phi\rangle_2 \end{bmatrix}. \tag{4}$$

This state definition also aids in simplifying the model description since the terms in (1) involving distributed delays are embedded in the states in (4), which yields a system description with only point-wise delays. By including the average inclination variables, as defined in Equation (2) in the states, the distributed delay terms present in the model in Section 2.1

can be avoided, and the model only contains terms related to point-wise delays in these new states. As a consequence of this model reformulation, four additional poles at zero are introduced. These additional poles can be disregarded in the stability analysis and stabilizing controller design[16] for the system as these are inconsequential for the original model described by (1). Now, the equations for the neutral bit walk model, ie, considering the model in (1) for the two-stabilizer case and with $\varpi = 0°$, can be rewritten in terms of the states defined in (4) as follows:

$$\begin{bmatrix} x'_\Theta \\ x'_\Phi \end{bmatrix} = \begin{bmatrix} A_0 & 0 \\ 0 & A_0 \end{bmatrix} \begin{bmatrix} x_\Theta(\xi) \\ x_\Phi(\xi) \end{bmatrix} + \begin{bmatrix} A_1 & 0 \\ 0 & A_1 \end{bmatrix} \begin{bmatrix} x_\Theta(\xi_1) \\ x_\Phi(\xi_1) \end{bmatrix} + \begin{bmatrix} A_2 & 0 \\ 0 & A_2 \end{bmatrix} \begin{bmatrix} x_\Theta(\xi_2) \\ x_\Phi(\xi_2) \end{bmatrix}$$
$$+ \begin{bmatrix} B_{0\Theta} & 0 \\ 0 & B_{0\Phi} \end{bmatrix} \begin{bmatrix} \Gamma_\Theta \\ \Gamma_\Phi \end{bmatrix} + \begin{bmatrix} B_{1\Theta} & 0 \\ 0 & B_{1\Phi} \end{bmatrix} \begin{bmatrix} \Gamma'_\Theta \\ \Gamma'_\Phi \end{bmatrix} + \begin{bmatrix} BW \\ 0 \end{bmatrix}, \tag{5}$$

where the matrices and vectors $A_0, A_1, A_2, B, B_{0i}, B_{1i}$, for $i = \Theta, \Phi$, are given by

$$A_0 = \frac{1}{\chi\Pi} \begin{bmatrix} -\mathcal{M}_b + \frac{\chi}{\eta}(\mathcal{F}_b - \mathcal{F}_1) & \mathcal{M}_b - \mathcal{M}_1 + \frac{\mathcal{F}_b\mathcal{M}_1 - \mathcal{F}_1\mathcal{M}_b}{\eta\Pi} & \mathcal{M}_1 + \frac{(-\mathcal{F}_b\mathcal{M}_1 + \mathcal{F}_1\mathcal{M}_b)}{\eta\Pi} \\ \chi\Pi & 0 & 0 \\ 0 & 0 & 0 \end{bmatrix}, \tag{6a}$$

$$A_1 = \frac{1}{\chi\Pi} \begin{bmatrix} \frac{\chi}{\eta}\left(\mathcal{F}_1 + \frac{\mathcal{F}_1}{\varkappa_2} - \mathcal{F}_b\right) & 0 & 0 \\ -\chi\Pi & 0 & 0 \\ \frac{\chi\Pi}{\varkappa_2} & 0 & 0 \end{bmatrix}, \qquad A_2 = \frac{1}{\chi\Pi} \begin{bmatrix} -\frac{\chi\mathcal{F}_1}{\eta\varkappa_2} & 0 & 0 \\ 0 & 0 & 0 \\ -\frac{\chi\Pi}{\varkappa_2} & 0 & 0 \end{bmatrix}, \tag{6b}$$

$$B_{0\Theta} = \frac{1}{\chi\Pi}\left[-\frac{\mathcal{M}_b\mathcal{F}_r + (\eta\Pi - \mathcal{F}_b)\mathcal{M}_r}{\eta\Pi},\ 0,\ 0 \right]^T, \qquad B_{1\Theta} = \frac{1}{\chi\Pi}\left[-\frac{\chi}{\eta}\mathcal{F}_r,\ 0,\ 0 \right]^T, \tag{6c}$$

$$B_{0\Phi} = \frac{1}{\chi\Pi}\left[\frac{\chi}{\eta}\frac{\mathcal{F}_r\Theta'\cos\Theta}{(\sin\Theta)^2} - \frac{\mathcal{M}_b\mathcal{F}_r + \mathcal{M}_r(\eta\Pi - \mathcal{F}_b)}{\eta\Pi\sin\Theta},\ 0,\ 0 \right]^T, \tag{6d}$$

$$B_{1\Phi} = \frac{1}{\chi\Pi}\left[-\frac{\chi}{\eta}\frac{\mathcal{F}_r}{\sin\Theta},\ 0,\ 0 \right]^T, \qquad B = \begin{bmatrix} 1 & 0 & 0 \end{bmatrix}^T, \tag{6e}$$

where the term related to the weight of the BHA (considered as slowly varying for an increasing length of the borehole disturbance) is included in Equation (5) through the term $W := -\frac{\mathcal{M}_b\mathcal{F}_w + (\eta\Pi - \mathcal{F}_b)\mathcal{M}_w}{\eta\Pi}\Upsilon\sin\langle\Theta\rangle_1 - \frac{\chi}{\eta}\mathcal{F}_w(\Theta - \Theta_1)\Upsilon\cos\langle\Theta\rangle_1$ and $\Theta_i := \Theta(\xi_i)$ and $\Phi_i := \Phi(\xi_i)$, with ξ_i being the location of the ith stabilizer of the BHA defined earlier. This model in terms of nonlinear delay differential equations will be used as a basis for controller design; nevertheless, in the simulation studies in Section 6, the non-neutral bit walk model (see (1) or (3)) will be used. Although the structure of the matrices in (5) may suggest decoupling of the inclination and azimuth dynamics, we care to stress that, in fact, nonlinear coupling from the inclination to the azimuth dynamics is still present through the Θ-dependent terms in the matrices $B_{0\Phi}$ and $B_{1\Phi}$.

Output equations

Measurements of the orientation of the borehole at the bit are not directly available in practice. Instead, inclination and azimuth are measured at specific locations on the BHA. A common location for these orientation sensors is one placed between the RSS and the bit and a second one between the first and second stabilizers. Using this knowledge, explicit expressions for the orientation of the BHA y_θ and y_ϕ (at the sensor locations) can be directly obtained from the BHA model, and the output equations of the system read as follows:

$$y_\theta = C_\Theta x_\Theta + D_\Theta\Gamma_\Theta + E\Upsilon\sin\langle\Theta\rangle_1, \tag{7a}$$

$$y_\phi = C_\Phi x_\Phi + D_\Phi\frac{\Gamma_\Phi}{\sin\Theta}, \tag{7b}$$

where the matrices C_i, D_i, and E, for $i = \Theta, \Phi$, depend on the location of the sensors and the configuration of the BHA. If it is assumed that both the inclination and azimuth sensors are at the same location, then $C_\Theta = C_\Phi$ and $D_\Theta = D_\Phi$. These matrix coefficients are again rather complex, and explicit expressions are omitted here for the sake of brevity and can be found explicitly in the work of Monsieurs.[21]

It is worth noting that there exists a singularity at the inclination of $\Theta = 0°$ in Equations (5) and (7), specifically in the terms $B_{0\Phi}$ and $B_{1\Phi}$ and in the equation that defines y_{Φ}. This singularity is related to the chosen orientation coordinates for the model (using inclination and azimuth) and not to a physical effect. We have opted for this coordinate description as it is widely used in the (directional) drilling industry.

3 | CONTROL PROBLEM FORMULATION

The main purpose of a directional drilling system is to drill a borehole with a predefined trajectory resulting in the desired borehole path. This trajectory is usually composed of different segments of constant curvature in both planes corresponding to the inclination and azimuth. In practice, it is often assumed that applying a constant force to the RSS actuators will lead to a constant curvature. This type of actuation can be considered as open-loop actuation, and the effects of its usage will be studied in this section. It has been shown before (see the works of Kremers et al[15] and van de Wouw et al[17]) that, due to the complex dynamics of the process, using open-loop actuation can potentially lead to oscillatory behavior (ie, borehole spiraling) of the borehole evolution. Hence, we formulate the generation of a complex 3D borehole geometry as a closed-loop reference tracking problem.

3.1 | Benchmark study

In order to perform simulation studies, we present a parameter set that defines a benchmark system representing a directional drilling system. Using the two-stabilizer system, the parameters are chosen based on the works of Perneder,[12] Monsieurs,[21] and Kremers.[25]

The BHA is considered to be made of steel pipes. The key properties of the system are Young's modulus (E_y), density (ρ), inner (I_r) and outer (O_r) radii of the BHA pipes, their cross-sectional surface area ($A = \pi(O_r^2 - I_r^2)$) and the second moment of inertia ($I = \frac{\pi}{4}(O_r^4 - I_r^4)$), the distance of the bit to the first stabilizer (ℓ_1), the distance of the second stabilizer with respect to the first (ℓ_2), and the distance of the RSS actuator from the bit, expressed as a fraction of ℓ_1 ($\Lambda\ell_1$) (see Figure 1). The parameter settings are shown in Tables C1 and C2. Using this set of parameters, the distributed weight of the BHA can be computed as $w = 9.81\pi\rho(O_r^2 - I_r^2) = 1.08 \times 10^3$ N/m. The chosen values for η and χ correspond to a bit with a rather long passive gauge. The active weight on bit Π and the bit walk angle ϖ are not given, since these parameters are considered uncertain (the effect of these parameters is analyzed in further sections); although, for Π, a "nominal" value of $\bar{\Pi} = \frac{14000[N]}{F^*}$ is used for controller design. Table C3 shows the values for the dimensionless parameters used for simulation. This set of parameters was chosen based on the work of Marck et al[4] and considered to reflect a real scenario of directional drilling.

3.2 | Open-loop dynamics

In this section, the behavior of the system described in Equation (5) when implementing a constant RSS actuator force (in this case, $\Gamma_\Theta = \Gamma_\Phi = 0.0074$) is evaluated. The initial conditions for these simulations are set to be $\Theta = 20°$ and $\Phi = 0°$.

Figure 4 (two left panels) shows the behavior of the system for several values of active weight on bit Π, considering $\varpi = 0°$. It can be noted that as the value of Π decreases, the system exhibits an instability leading to oscillations (borehole spiraling). This Figure shows that for a higher weight on bit, these oscillations disappear. In such cases, a drift in the inclination and azimuth is apparent. Finally, Figure 4 also shows the stepwise sudden change in inclination and azimuth due to a constant applied RSS actuator force (which can be seen at $\xi = 0$ in Figure 4). This produces a kink in the borehole, which is undesirable in practice.

The two right panels in Figure 4 show the effect of a nonzero bit walk angle on the system response (note that, here, $\Pi = 0.0087$, such that for zero bit walk, no oscillations occur; see left panels in Figure 4). Clearly, a higher (absolute value of the) bit walk angle leads to oscillations, even for a level of the weight on bit for which no oscillations occur for a zero bit walk angle. This undesired bit walk–induced instability is related to nonlinear coupling terms in the system dynamics in which the bit walk effect plays a role. When the bit walk angle is not severe, after some oscillations, the inclination and azimuth start to grow linearly (ie, a constant curvature is generated) for this weight on bit of $\Pi = 0.0087$. As mentioned before, as the absolute value of ϖ increases, the response becomes more oscillatory, and in the severe case of $\varpi = \pm 40°$, the system is close to instability. It can be seen that there is a symmetric behavior in terms of ϖ, since all the terms in

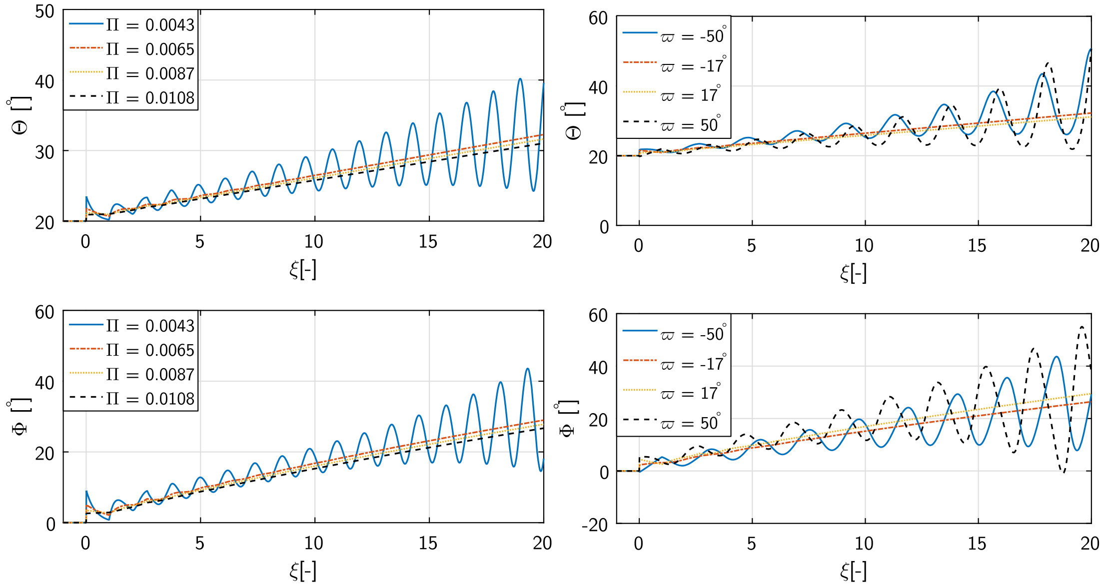

FIGURE 4 Open-loop response of Θ and Φ for different values of weight on bit Π and $\varpi = 0°$ (left) and bit walk angle ϖ and $\Pi = 0.0087$ (right) [Colour figure can be viewed at wileyonlinelibrary.com]

which the bit walk angle ϖ is present are sine or cosine functions. This could be insightful for the robust controller design to reduce the range of parameters for which a robust controller strategy could be designed.

This oscillatory behavior was observed in the works of Marck et al,[4] Perneder and Detournay,[18] Detournay et al,[26] and Marck and Detournay,[27] and one of the main goals of this work is avoiding the borehole spiraling effect displayed in Figure 4 by means of control. These results highlight the fact that open-loop actuation cannot guarantee the desired behavior of the directional drilling system and motivates the design of a feedback control system. Moreover, recalling the fact that the weight on bit and the bit walk angle are typically uncertain in practice and given the sensitivity of the system dynamics to these parameters (see Figure 4), we conclude that a robust control strategy is required.

3.3 | Control approach

The main goal of directional drilling is the generation of a borehole with some desired complex 3D geometry. In terms of the model in (5) (or (3) in the non-neutral bit walk case), this objective can be formulated as a tracking problem. More specifically, we aim to track the inclination and azimuth reference trajectory $(\Theta_r(\xi), \Phi_r(\xi))$, for $\xi \in [-\varkappa_{\text{tot}}, \infty]$. We assume that $\Theta_r(\xi)$ and $\Phi_r(\xi)$ are continuously differentiable, which is reasonable at the scale at which the problem is treated as it avoids curvature discontinuities. We aim to design a dynamic output-feedback controller such that the control inputs $\Gamma_i(\xi), i = \Theta, \Phi$, render $(\Theta_r(\xi), \Phi_r(\xi))$ the asymptotically stable solution of the closed-loop system.

In addition, certain additional control objectives stem from the fact that the spiraling behavior in the borehole, which is often observed in practice, needs to be reduced/eliminated. Such borehole spiraling is caused by directional instability of the system (see, eg, Figure 4), which is avoided if the tracking problem is solved. For this reason, we also focus on achieving improved transient behavior in order to reduce/eliminate transient borehole spiraling. Another control objective is related to the rejection of slowly changing gravity-induced forces. Finally, the control strategy to be proposed in the next sections, should exhibit favorable robustness properties against uncertainties in the weight on bit and the bit walk angle. To summarize, the list of the control objectives is provided as follows.

1. Track an inclination and azimuth reference trajectory $(\Theta_r(\xi), \Phi_r(\xi))$.
2. Reduce/eliminate borehole spiraling behavior.
3. Rejection of slowly varying gravity-induced force disturbances W.
4. Robustness against parameter uncertainty in the weight on bit Π and the bit walk angle ϖ.

4 | CONTROLLER DESIGN

In this section, a controller design based on the neutral bit walk model is developed. Let us first discuss the importance of the different "length" (ξ) scales present in the directional drilling model. They characterize the phenomena occurring at *short* length scales (related to fast geometrical changes, such as borehole kinking), *medium* length scales (related to borehole oscillations), and *long* length scales (related to steady-state inclination). The controller design explicitly takes these different length scales into account, as explained in detail in Remark 4 below.

The control strategy should rely only on the local measurements of the BHA inclination and azimuth. However, the control goal is the stabilization of a desired trajectory in terms of the inclination and azimuth of the *borehole*, not that of the BHA. Indeed, the inclination and azimuth of the BHA at the bit differ from those of the borehole due to the deflection of the BHA caused by the RSS force and gravity. Note that the deflection of the BHA is, in fact, key to the directional tendency of the borehole. Moreover, the inclination and azimuth of the BHA cannot even be measured at the bit but only at some distance behind the bit. In order to cope with these sensor constraints, we aim to design an observer that estimates the inclination and azimuth of the borehole at the bit based on the model and measurements of the inclination and azimuth of the BHA at some distance behind the bit. Next, a combined feedforward and feedback control strategy is developed, which employs the state estimates provided by the observer and asymptotically stabilizes the desired trajectory.

Before explaining each of the elements that comprise the proposed control strategy, we summarize a list of assumptions and properties that will be useful for controller design and derivations in this section and in Section 5.

Assumption 1. Without loss of generality, the control strategy is described here for the two-stabilizer case, since it captures the key dynamics of the process (see the work of Marck et al[4]).

Assumption 2. For the equilibrium points (both in the nominal and robust cases), we assume that the influence of the gravitational term in the output equations (7) is $W_y = 0$ since it generally has a very small influence on the overall system dynamics (see the work of Kremers et al[15]).

Assumption 3. In the case of the equilibrium points of the closed-loop dynamics for robust controller design, the equilibrium point is chosen to be the same as in the nominal case, despite the fact that the equilibrium solution yields a ξ-dependent solution. This assumption is explained in further detail in Section 5.

Assumption 4. Neutral bit walk tendency ($\varpi = 0°$). That is, the model used as basis for controller design is the one described by Equation (5).

4.1 | Controller structure

Figure 5 depicts the proposed control strategy for the system. The controller consists of (i) a combined feedforward and state-feedback tracking controller, (ii) a state observer, (iii) an input filter, and (iv) a nonlinear input decoupling transformation. These controller elements will be explained in detail subsequently.

Decoupling input transformation

The following input transformation is proposed in order to achieve decoupling of the system between the inclination and azimuth dynamics:

$$\begin{bmatrix} \Gamma_\Theta^* \\ \Gamma_\Phi^* \end{bmatrix} := \begin{bmatrix} 1 & 0 \\ 0 & \frac{1}{\sin\check{\Theta}} \end{bmatrix} \begin{bmatrix} \Gamma_\Theta \\ \Gamma_\Phi \end{bmatrix}, \qquad \text{for } \Theta \in (0,\ \pi). \tag{8}$$

We denote the observer estimate of a state using the character ($\check{}$). Herein, $\check{\Theta}$ denotes the estimate of the inclination Θ of the borehole at the bit, which will be provided by an observer to be designed below (recall that Θ cannot be measured in practice).

In terms of the states defined in (4), the system dynamics after the decoupling input transformation can be written as

$$\begin{aligned} \begin{bmatrix} x'_\Theta \\ x'_\Phi \end{bmatrix} &= \begin{bmatrix} A_0 & 0 \\ 0 & A_0 \end{bmatrix} \begin{bmatrix} x_\Theta(\xi) \\ x_\Phi(\xi) \end{bmatrix} + \begin{bmatrix} A_1 & 0 \\ 0 & A_1 \end{bmatrix} \begin{bmatrix} x_\Theta(\xi_1) \\ x_\Phi(\xi_1) \end{bmatrix} + \begin{bmatrix} A_2 & 0 \\ 0 & A_2 \end{bmatrix} \begin{bmatrix} x_\Theta(\xi_2) \\ x_\Phi(\xi_2) \end{bmatrix} \\ &+ \begin{bmatrix} B_{0\Theta} & 0 \\ 0 & \tilde{B}_{0\Phi} \end{bmatrix} \begin{bmatrix} \Gamma_\Theta^* \\ \Gamma_\Phi^* \end{bmatrix} + \begin{bmatrix} B_{1\Theta} & 0 \\ 0 & \tilde{B}_{1\Phi} \end{bmatrix} \begin{bmatrix} \Gamma_\Theta^{*\prime} \\ \Gamma_\Phi^{*\prime} \end{bmatrix} + \begin{bmatrix} BW \\ 0 \end{bmatrix}, \end{aligned} \tag{9}$$

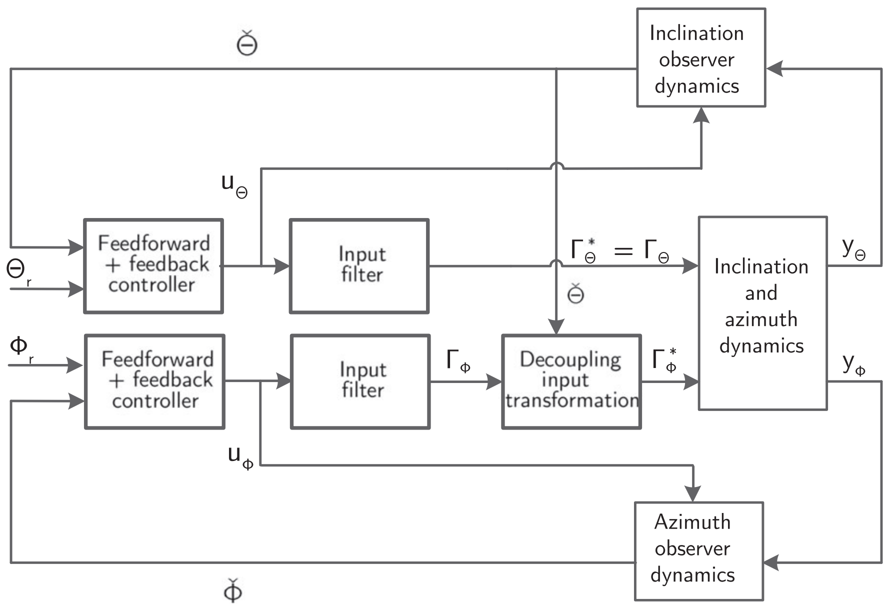

FIGURE 5 Structure of the proposed control strategy

with the vectors $\tilde{B}_{0\Phi}$ and $\tilde{B}_{1\Phi}$ given by

$$\tilde{B}_{0\Phi} = \frac{1}{\chi\Pi}\left[\frac{\chi}{\eta}\frac{\mathcal{F}_r\Theta'\cos\Theta\sin\check{\Theta}}{(\sin\Theta)^2} - \frac{\left(\mathcal{M}_b\mathcal{F}_r+\mathcal{M}_r(\eta\Pi-\mathcal{F}_b)\right)\sin\check{\Theta}}{\eta\Pi\sin\Theta} - \frac{\chi}{\eta}\frac{\mathcal{F}_r\check{\Theta}'\cos\check{\Theta}}{(\sin\Theta)},\ 0,\ 0\right]^T \tag{10a}$$

$$\tilde{B}_{1\Phi} = \frac{1}{\chi\Pi}\left[-\frac{\chi}{\eta}\mathcal{F}_r\frac{\sin\check{\Theta}}{\sin\Theta},\ 0,\ 0\right]^T. \tag{10b}$$

After the input transformation, the output equations in (7a) and (7b) are given by

$$y_\theta = C_\Theta x_\Theta + D_\Theta \Gamma^*_\Theta + EW_y, \tag{11a}$$

$$y_\phi = C_\Phi x_\Phi + D_\Phi \Gamma^*_\Phi \frac{\sin\check{\Theta}}{\sin\Theta}, \tag{11b}$$

where the gravity-related term in y_Θ has been renamed EW_y, with $W_y := \Upsilon \sin\langle\Theta\rangle_1$ to simplify notation. We emphasize again that we consider W and W_y as slowly varying disturbances.

Remark 1. *Decoupling*: Note that if $\check{\Theta} = \Theta$ (a perfect estimate), then (8) indeed fully decouples the azimuth dynamics from the inclination dynamics. Note that in such a case, $\tilde{B}_{0\Phi}$ and $\tilde{B}_{1\Phi}$ are independent of Θ and $\check{\Theta}$, and this simplifies the design of the structure of the controller and the observer. However, in general, $\check{\Theta} \neq \Theta$ (at least in transients of the observer), and the mismatch between Θ and $\check{\Theta}$ affects the decoupling transformation.

Remark 2. *Nonlinearities*: The borehole propagation model exhibits nonlinearities on three levels: (i) nonlinear coupling through RSS force terms (this nonlinearity is linearized when $\check{\Theta} = \Theta$; see Remark 1), (ii) nonlinear gravity effects (which are considered as a (slowly varying) constant disturbance), and (iii) nonlinearities due to the bit walk effect (not present in the neutral bit walk case). Hence, the dynamics in (9) will be linear once the condition $\check{\Theta} = \Theta$ is met.

Input filters

In support of the tracking controller design, discussed in the next section, input filters (see Figure 5) are included in the design. The (transformed) RSS force inputs Γ^*_i, for $i = \Theta, \Phi$, and their derivatives are combined via the following transformations:

$$Bu_\Theta = B_{0\Theta}\Gamma^*_\Theta + B_{1\Theta}\Gamma^{*\prime}_\Theta, \qquad Bu_\Phi = \tilde{B}_{0\Phi}\Gamma^*_\Phi + \tilde{B}_{1\Phi}\Gamma^{*\prime}_\Phi, \tag{12}$$

with u_Θ and u_Φ as the new control inputs and where $B = [\,1\ 0\ 0\,]^T$.

The input filter design in (12) would fully replace the terms related to Γ^*_i, for $i = \Theta, \Phi$, and their derivatives in the dynamics given by (9) with Bu_Θ and Bu_Φ. However, the input filter as in (12) cannot be implemented, since vectors $\tilde{B}_{0\Phi}$

and $\tilde{B}_{1\Phi}$ depend on Θ, which is not known to the controller, since it cannot be measured. To overcome this problem, the design of this input filter will be performed for the ideal case when $\check{\Theta} = \Theta$, ie,

$$\Gamma_i^{*'} = -\frac{\mathcal{M}_b\mathcal{F}_r + (\eta\Pi - \mathcal{F}_b)\mathcal{M}_r}{\chi\Pi\mathcal{F}_r}\Gamma_i^* - \frac{\eta\Pi}{\mathcal{F}_r}u_i, \qquad \text{for } i = \Theta, \Phi. \tag{13}$$

Tracking controller

In (13), u_i is comprised of the sum of the feedforward and feedback inputs, u_{ri} and v_i, respectively, given by

$$u_i = v_i + u_{ri}. \tag{14}$$

The tracking controller defined by the control input given in (14) is comprised of the feedforward input defined based on the inverse dynamics of the system for a reference trajectory x_{ri}, for $i = \Theta, \Phi$, ie,

$$u_{ri} = B^T \left(x'_{ri}(\xi) - A_0 x_{ri}(\xi) - A_1 x_{ri}(\xi_1) - A_2 x_{ri}(\xi_2)\right), \tag{15}$$

where the reference vector is defined as $x_{ri} = [\, i_r \ \langle i \rangle_{r1} \ \langle i \rangle_{r2} \,]$, for $i = \Theta, \Phi$.

Remark 3. *Feedforward*: It is important to mention that the gravity-related term in the inclination dynamics (W in (5)) is omitted from the feedforward design since it can be considered as a slowly varying (though unknown) disturbance, which can be dealt with by implementing an integral action in the control structure. Furthermore, this feedforward is designed also for the case when $\check{\Theta} = \Theta$. Due to this simplification of the feedforward design, a (transient) feedforward error is introduced to the system, which will be taken into account explicitly in the resulting error dynamics and stability analysis presented later. The state-feedback controller corresponds to the input v_i acting on the difference between the estimate of the state vector $\check{x}_i$ (which is obtained via the observer defined below) and the reference vector x_{ri}. A dynamic state-feedback controller is designed as follows:

$$z'_{1i} = \zeta_c \left[\, k_{1i} \ 0 \ 0 \,\right] (\check{x}_i - x_{ri}) \tag{16a}$$

$$z'_{2i} = -\gamma z_{2i} + \gamma \left(z_{1i} + K_i(\check{x}_i - x_{ri})\right) \tag{16b}$$

$$v_i = z_{2i}, \tag{16c}$$

for $i = \Theta, \Phi$. This controller consists of a static state-feedback part (with proportional gain $K_i = [\, k_{1i} \ k_{2i} \ k_{3i} \,]$), a low-pass filter (with cutoff frequency determined by gain γ), and an integral action (with cutoff frequency determined by gain ζ_c). The low-pass filter is used in order to prevent fast changes in the response of the system, since these produce what is called borehole kinking. The purpose of the integral action is to reject the influence of the gravity-related terms in the inclination dynamics (as they are considered a slowly varying disturbance).

Observer design

Considering the fact that the states cannot be measured directly and the state estimate $\check{x}_i$, for $i = \Theta, \Phi$, is used in the tracking controller in (16), an observer is designed in order to support the implementation of the state-feedback controller in (16). Since the weight of the BHA is taken into account as a slowly varying disturbance, an integral action is also included in the observer design. The integral action of the observer is embedded through the integral filter, ie,

$$q'_i = \zeta_o[l_1, l_2](y_i - \check{y}_i), \qquad \text{for } i = \Theta, \Phi, \tag{17}$$

with the estimated output $\check{y}_i$ defined below. The observer consists of a model-based (predictor) part and an output-injection part. The predictor part of the observer is designed by again considering the model under the condition that $\Theta = \check{\Theta}$. In total, the dynamics of the observer with an integral action are given by

$$\begin{bmatrix} \check{x}'_\Theta \\ q'_\Theta \\ \check{x}'_\Phi \\ q'_\Phi \end{bmatrix} = \begin{bmatrix} A_0 & 0 & 0 & 0 \\ 0 & 0 & 0 & 0 \\ 0 & 0 & A_0 & 0 \\ 0 & 0 & 0 & 0 \end{bmatrix} \begin{bmatrix} \check{x}_\Theta(\xi) \\ q_\Theta(\xi) \\ \check{x}_\Phi(\xi) \\ q_\Phi(\xi) \end{bmatrix} + \begin{bmatrix} A_1 & 0 & 0 & 0 \\ 0 & 0 & 0 & 0 \\ 0 & 0 & A_1 & 0 \\ 0 & 0 & 0 & 0 \end{bmatrix} \begin{bmatrix} \check{x}_\Theta(\xi_1) \\ q_\Theta(\xi_1) \\ \check{x}_\Phi(\xi_1) \\ q_\Phi(\xi_1) \end{bmatrix}$$
$$+ \begin{bmatrix} A_2 & 0 & 0 & 0 \\ 0 & 0 & 0 & 0 \\ 0 & 0 & A_2 & 0 \\ 0 & 0 & 0 & 0 \end{bmatrix} \begin{bmatrix} \check{x}_\Theta(\xi_2) \\ q_\Theta(\xi_2) \\ \check{x}_\Phi(\xi_2) \\ q_\Phi(\xi_2) \end{bmatrix} + \begin{bmatrix} L_\Theta(y_\Theta - \check{y}_\Theta) \\ \zeta_o[l_{1\Theta}, l_{2\Theta}](y_\Theta - \check{y}_\Theta) \\ L_\Phi(y_\Phi - \check{y}_\Phi) \\ \zeta_o[l_{1\Phi}, l_{2\Phi}](y_\Phi - \check{y}_\Phi) \end{bmatrix} + \begin{bmatrix} Bq_\Theta \\ 0 \\ Bq_\Phi \\ 0 \end{bmatrix} + \begin{bmatrix} B(u_{r\Theta} + v_\Theta) \\ 0 \\ B(u_{r\Phi} + v_\Phi) \\ 0 \end{bmatrix}, \tag{18}$$

where L_i is defined as

$$L_i = \begin{bmatrix} l_{1i} & l_{2i} \\ 0 & 0 \\ 0 & 0 \end{bmatrix}, \qquad \text{for } i = \Theta, \Phi, \tag{19}$$

and with the observer output equations (taking into account the ideal input decoupling transformation) given by

$$\check{y}_\Theta = C_\Theta \check{x}_\Theta + D_\Theta \Gamma^*_\Theta \tag{20a}$$

$$\check{y}_\Phi = C_\Phi \check{x}_\Phi + D_\Phi \Gamma^*_\Phi. \tag{20b}$$

Remark 4. The dynamics of the directional drilling model exhibit three essential length scales: (i) short range, $\xi = O(10^{-1})$, related to fast geometrical changes (borehole kinking) induced by changes in the RSS force; (ii) medium range, $\xi = O(10^0 - 10^1)$, related to borehole oscillations; and (iii) long range, $\xi = O(10^2 - 10^3)$, related to the steady-state inclination behavior (see the work of Perneder and Detournay[18]).

The structural design of the controller proposed above targets these different length scales in the following way.

- Short range: the low-pass filtering properties in the feedback controller (16) (determined by γ) ensure that the excitation of the short-range (boundary layer) dynamics is avoided, therewith avoiding severe borehole kinking.
- Medium range: the design of both the observer in (18) and the controller in (16) aims at the stabilization of the medium-range dynamics (through design of the gains L_i and K_i), therewith guaranteeing the generation of a desired borehole geometry and the absence of instabilities related to borehole oscillations.
- Long range: the inclusion of an integral action in the controller in both the observer in (18) and the controller in (16) (determined by ζ_c and ζ_o) ensures the long-range tracking error to be zero in the presence of (eg, gravity-related) disturbances.

4.2 | Analysis of the closed-loop tracking error dynamics

In this section, the equations for the closed-loop error dynamics are provided, which will be used to support the design of the controller and observer gains.

The tracking and observer errors are defined as $e_i = x_i - x_{ri}$ and $\delta_i = x_i - \check{x}_i$, for $i = \Theta, \Phi$, respectively. Furthermore, the error coordinates for the transformed RSS force inputs are introduced. In order to do so, an input filter as in Equation (13) is designed based on the feedforward input, ie,

$$\Gamma^{*\prime}_{\text{id}} = -\frac{\mathcal{M}_b \mathcal{F}_r + (\eta\Pi - \mathcal{F}_b)}{\chi \Pi \mathcal{F}_r} \Gamma^*_{\text{id}} - \frac{\eta\Pi}{\mathcal{F}_r} u_{ri}, \tag{21}$$

where Γ^*_{id} is a desired input of the RSS corresponding to the feedforward input. Then, an error coordinate for the transformed input Γ^*_i can be defined as $\Delta\Gamma^*_i = \Gamma^*_i - \Gamma^*_{\text{id}}$.

Then, if the elements of the controller structure (decoupling input transformation, input filters, tracking controller, state-feedback controller and observer) are introduced into the closed-loop error dynamics and considering the fact that $\check{x}_i - x_{ri} = e_i - \delta_i$ and $\Gamma^*_i = \Delta\Gamma^*_i + \Gamma^*_{\text{id}}$, for $i = \Theta, \Phi$, the state vector can be defined as

$$X(\xi) = \begin{bmatrix} X_\Theta(\xi) \\ X_\Phi(\xi) \end{bmatrix}, \tag{22}$$

with

$$X_i(\xi) = \left[e_i^T(\xi) \quad \Delta\Gamma_i^*(\xi) \quad z_{1i}(\xi) \quad z_{2i}(\xi) \quad \delta_i^T(\xi) \quad q_i(\xi) \right]^T,$$

for $i = \Theta, \Phi$. Then, the total error dynamics are given by

$$X'(\xi) = A_{0\mathrm{cl}}X(\xi) + A_{1\mathrm{cl}}X(\xi_1) + A_{2\mathrm{cl}}X(\xi_2) + P_{\mathrm{cl}}\left(u_{r\Phi}, \Gamma_{\Phi d}^*, \alpha, \Theta, \check{\Theta}, W\right), \tag{23}$$

where the subscript "cl" stands for "closed-loop" and matrices $A_{0\mathrm{cl}}, A_{1\mathrm{cl}}$, and $A_{2\mathrm{cl}}$ are given by

$$A_{0\mathrm{cl}} = \begin{bmatrix} A_{0\Theta} & 0 \\ 0 & A_{0\Phi} \end{bmatrix}, \qquad A_{1\mathrm{cl}} = \begin{bmatrix} A_{1\Theta} & 0 \\ 0 & A_{1\Phi} \end{bmatrix}, \qquad A_{2\mathrm{cl}} = \begin{bmatrix} A_{2\Theta} & 0 \\ 0 & A_{2\Phi} \end{bmatrix}, \tag{24}$$

where the system matrices in (24) and the vector P_{cl} are given by

$$A_{0\Theta} = \left[\begin{array}{cccc:cc} A_0 & 0 & 0 & B & 0 & 0 \\ 0 & -b_0 & 0 & -b_1 & 0 & 0 \\ \zeta\left[k_{1\Theta}, 0, 0\right] & 0 & 0 & 0 & -\zeta\left[k_{1\Theta}, 0, 0\right] & 0 \\ \gamma K_\Theta & 0 & \gamma & -\gamma & -\gamma K_\Theta & 0 \\ \hdashline 0 & 0 & 0 & 0 & A_0 - L_\Theta C_\Theta & -B \\ 0 & 0 & 0 & 0 & \zeta\left[l_{1\Theta}, l_{2\Theta}\right] C_\Theta & 0 \end{array}\right],$$

$$A_{0\Phi} = \left[\begin{array}{cccc:cc} A_0 & B\alpha & 0 & B\left(\frac{\sin\check{\Theta}}{\sin\Theta}\right) & 0 & 0 \\ 0 & -b_0 & 0 & -b_1 & 0 & 0 \\ \zeta\left[k_{1\Phi}, 0, 0\right] & 0 & 0 & 0 & -\zeta\left[k_{1\Phi}, 0, 0\right] & 0 \\ \gamma K_\Phi & 0 & \gamma & -\gamma & -\gamma K_\Phi & 0 \\ \hdashline 0 & B\alpha - L_\Phi D_\Phi\left(\frac{\sin\check{\Theta}}{\sin\Theta} - 1\right) & 0 & B\left(\frac{\sin\check{\Theta}}{\sin\Theta} - 1\right) & A_0 - L_\Phi C_\Phi & -B \\ 0 & \zeta\left[l_{1\Phi}, l_{2\Phi}\right] D_\Phi\left(\frac{\sin\check{\Theta}}{\sin\Theta} - 1\right) & 0 & 0 & \zeta\left[l_{1\Phi}, l_{2\Phi}\right] C_\Phi & 0 \end{array}\right],$$

$$A_{1i} = \left[\begin{array}{cccc:cc} A_1 & 0 & 0 & 0 & 0 & 0 \\ 0 & 0 & 0 & 0 & 0 & 0 \\ 0 & 0 & 0 & 0 & 0 & 0 \\ 0 & 0 & 0 & 0 & 0 & 0 \\ \hdashline 0 & 0 & 0 & 0 & A_1 & 0 \\ 0 & 0 & 0 & 0 & 0 & 0 \end{array}\right], \quad A_{2i} = \left[\begin{array}{cccc:cc} A_2 & 0 & 0 & 0 & 0 & 0 \\ 0 & 0 & 0 & 0 & 0 & 0 \\ 0 & 0 & 0 & 0 & 0 & 0 \\ 0 & 0 & 0 & 0 & 0 & 0 \\ \hdashline 0 & 0 & 0 & 0 & A_2 & 0 \\ 0 & 0 & 0 & 0 & 0 & 0 \end{array}\right],$$

$$P_{\mathrm{cl}}\left(u_{r\Phi}, \Gamma_{\Phi d}^*, \alpha, \Theta, \check{\Theta}, W\right) = \left[\begin{array}{c} BW \\ 0 \\ 0 \\ 0 \\ \hdashline BW - L_\Theta E W_y \\ \zeta[l_{1\Theta}, l_{2\Theta}]EW_y \\ \hline B\left(\frac{\sin\check{\Theta}}{\sin\Theta} - 1\right)u_{r\Phi} + B\alpha(\Theta, \check{\Theta}, \Theta', \check{\Theta}')\Gamma_{\Phi d}^* \\ 0 \\ 0 \\ 0 \\ \hdashline B\left(\frac{\sin\check{\Theta}}{\sin\Theta} - 1\right)u_{r\Phi} + B\alpha(\Theta, \check{\Theta}, \Theta', \check{\Theta}')\Gamma_{\Phi d}^* - LD\left(\frac{\sin\check{\Theta}}{\sin\Theta} - 1\right)\Gamma_{\Phi d}^* \\ \zeta\left[l_{1\Phi}, l_{2\Phi}\right] D_\Phi\left(\frac{\sin\check{\Theta}}{\sin\Theta} - 1\right)\Gamma_{\Phi d}^* \end{array}\right]$$

and where

$$
b_0 = \frac{\mathcal{M}_b \mathcal{F}_r + (\eta\Pi - \mathcal{F}_b)\mathcal{M}_r}{\chi \Pi \mathcal{F}_r}, \quad b_1 = \frac{\eta \Pi}{\mathcal{F}_r},
$$
$$
\alpha(\Theta, \check{\Theta}, \Theta', \check{\Theta}') = \frac{\mathcal{F}_r}{\eta \Pi \sin \Theta} \left(\frac{\Theta' \cos \Theta \sin \check{\Theta}}{\sin \Theta} - \check{\Theta}' \cos \check{\Theta} \right). \tag{25}
$$

Note that $\alpha(\Theta, \check{\Theta}, \Theta', \check{\Theta}')$ depends on the states Θ and $\check{\Theta}$, and their derivatives. To simplify notation, we write α instead of $\alpha(\Theta, \check{\Theta}, \Theta', \check{\Theta}')$ from now on.

We observe that the vector P_{cl} contains the gravity-related terms, which were not included in the feedforward design. These terms in P_{cl} can be rejected by a dedicated integral action. Moreover, the other perturbation terms in P_{cl} vanish if $\check{\Theta} = \Theta$ (ie, if the inclination observer error is zero).

In the sequel, stability analysis and the synthesis of the controller and observer gains are performed using linearized system dynamics around an equilibrium point corresponding to zero tracking and observer error (ie, $e_i = \delta_i = 0$, for $i = \Theta, \Phi$). For the equilibrium point analysis, it is assumed that $W_y = 0$, since it has been noted that its influence is generally very small (including that this term may lead to an equilibrium solution where $\delta_\Theta \neq 0$, which is not desired; see Assumption 2). Also, Θ and $\check{\Theta}$ are expressed in terms of e_Θ, δ_Θ, and $x_{r\Theta}$ (see the work of Villarreal Magaña[22]). The equilibrium point is of the form

$$
\begin{aligned}
X_e :&= \left[e_{\Theta,e}^T \;\; \Delta\Gamma_{\Theta,e}^* \;\; z_{1\Theta,e} \;\; z_{2\Theta,e} \;\; \delta_{\Theta,e}^T \;\; q_{\Theta,e} \;\; e_{\Phi,e}^T \;\; \Delta\Gamma_{\Phi,e}^* \;\; z_{1\Phi,e} \;\; z_{2\Phi,e} \;\; \delta_{\Phi,e}^T \;\; q_{\Phi,e} \right]^T \\
&= \left[0^T \;\; \Delta\Gamma_{\Theta,e}^* \;\; z_{1\Theta,e} \;\; z_{2\Theta,e} \;\; 0^T \;\; q_{\Theta,e} \;\; 0^T \;\; 0 \;\; 0 \;\; 0 \;\; 0^T \;\; 0 \right]^T,
\end{aligned} \tag{26}
$$

where the subscript "e" stands for "equilibrium." The nonzero terms are caused by the influence of the gravity term W and for which the perturbed states $\Delta z_{1\Theta}$, $\Delta z_{2\Theta}$, Δq_Θ, and $\Delta\bar{\Gamma}_\Theta$ are introduced.

By introducing the perturbation state vector $\bar{X}(\xi)$ given by

$$
\bar{X}(\xi) = \left[e_\Theta^T(\xi) \;\; \Delta\bar{\Gamma}_\Theta^*(\xi) \;\; \Delta z_{1\Theta}(\xi) \;\; \Delta z_{2\Theta}(\xi) \;\; \delta_\Theta^T(\xi) \;\; \Delta q_\Theta(\xi) \;\; e_\Phi^T(\xi) \;\; \Delta\Gamma_\Phi^*(\xi) \;\; z_{1\Phi}(\xi) \;\; z_{2\Phi}(\xi) \;\; \delta_\Phi^T(\xi) \;\; q_\Phi(\xi) \right]^T,
$$

such that $X(\xi) = X_e + \bar{X}(\xi)$, the linearized system dynamics are given by

$$
\bar{X}'(\xi) = \bar{A}_{0\mathrm{cl}} \bar{X}(\xi) + \bar{A}_{1\mathrm{cl}} \bar{X}(\xi_1) + \bar{A}_{2\mathrm{cl}} \bar{X}(\xi_2), \tag{27}
$$

where the linearized matrices $\bar{A}_{0\mathrm{cl}}$, $\bar{A}_{1\mathrm{cl}}$, and $\bar{A}_{2\mathrm{cl}}$ are given by

$$
\bar{A}_{0\mathrm{cl}} = \begin{bmatrix} \bar{A}_{0\Theta} & 0 \\ \bar{A}_{0c} & \bar{A}_{0\Phi} \end{bmatrix}, \qquad \bar{A}_{1\mathrm{cl}} = \begin{bmatrix} \bar{A}_{1\Theta} & 0 \\ \bar{A}_{1c} & \bar{A}_{1\Phi} \end{bmatrix}, \qquad \bar{A}_{2\mathrm{cl}} = \begin{bmatrix} \bar{A}_{2\Theta} & 0 \\ \bar{A}_{2c} & \bar{A}_{2\Phi} \end{bmatrix}, \tag{28}
$$

with

$$
\begin{aligned}
\bar{A}_{0i} &= \left[\begin{array}{cccc|cc} A_0 & 0 & 0 & B & 0 & 0 \\ 0 & -b_0 & 0 & -b_1 & 0 & 0 \\ \zeta \left[k_{1i}, 0, 0 \right] & 0 & 0 & 0 & -\zeta \left[k_{1i}, 0, 0 \right] & 0 \\ \gamma K_i & 0 & \gamma & -\gamma & -\gamma K_i & 0 \\ \hline 0 & 0 & 0 & 0 & A_0 - L_i C_i & -B \\ 0 & 0 & 0 & 0 & \zeta \left[l_{1i}, l_{2i} \right] C_i & 0 \end{array} \right], \\
\bar{A}_{0c} &= \left[\begin{array}{cccc|cc} 0 & 0 & 0 & 0 & p_{0e1}(\xi) & p_{0e2}(\xi) \\ 0 & 0 & 0 & 0 & 0 & 0 \\ 0 & 0 & 0 & 0 & 0 & 0 \\ 0 & 0 & 0 & 0 & 0 & 0 \\ \hline 0 & 0 & 0 & 0 & p_{0\delta 1}(\xi) & p_{0\delta 2}(\xi) \\ 0 & 0 & 0 & 0 & p_{0q}(\xi) & 0 \end{array} \right], \\
\bar{A}_{ji} &= \left[\begin{array}{cccc|cc} A_j & 0 & 0 & 0 & 0 & 0 \\ 0 & 0 & 0 & 0 & 0 & 0 \\ 0 & 0 & 0 & 0 & 0 & 0 \\ 0 & 0 & 0 & 0 & 0 & 0 \\ \hline 0 & 0 & 0 & 0 & A_j & 0 \\ 0 & 0 & 0 & 0 & 0 & 0 \end{array} \right], \qquad \bar{A}_{jc} = \left[\begin{array}{cccc|cc} 0 & 0 & 0 & 0 & p_{je}(\xi) & 0 \\ 0 & 0 & 0 & 0 & 0 & 0 \\ 0 & 0 & 0 & 0 & 0 & 0 \\ 0 & 0 & 0 & 0 & 0 & 0 \\ \hline 0 & 0 & 0 & 0 & p_{j\delta}(\xi) & 0 \\ 0 & 0 & 0 & 0 & 0 & 0 \end{array} \right],
\end{aligned} \tag{29}
$$

for $i = \Theta, \Phi$ and $j = 1, 2$. The $p(\xi)$-coefficients in these linearized dynamics are related to the ξ-dependent reference trajectory. The exact values of these coefficients can be found in Appendix A.

Note that after the linearization, the nonlinear perturbation vector $P_{\rm cl}$, as in the nonlinear dynamics in (23), only yields terms that affect the $\bar{A}_{0c}$, $\bar{A}_{1c}$, and $\bar{A}_{2c}$ matrices above and does not introduce a perturbation term in the linearized dynamics in (27).

4.3 | Controller synthesis

In this section, the controller and observer gains will be synthesized. In Section 5, we study the robustness against uncertainty in the active weight on bit Π and propose a robust control strategy for a nominal parameter setting. It is worth noting that despite the fact that the nominal controller design is a specific case of the robust controller design (when Π is considered constant), we first present the analysis of the nominal controller design separately for several reasons. In particular, the study of the nominal case provides insight about the usefulness of the cascaded systems argument for the stability analysis of the error dynamics. In particular, we notice that in the nominal case, the structure of the closed-loop system matrices of Equation (27) allows us to exploit this cascaded systems argument and make use of the separation principle between controller and observer designs. It will be noted that the separation principle that holds in the nominal case is no longer valid in the robust case (see Figure 6). However, inspired by the analysis for the nominal case, the same type of cascaded systems argument can be used in the robust case, considering the coupling between error and observer error dynamics for both the inclination and the azimuth.

We note that the stabilizing gain design of the controller and observer is challenged by the fact that the linearized dynamics are ξ-dependent (ie, not "LTI").

We start the analysis by noting that the main diagonals of $\bar{A}_{\rm ocl}$, $\bar{A}_{\rm 1cl}$, and $\bar{A}_{\rm 2cl}$ in (27) have the same structure for both the inclination and azimuth dynamics. The matrices $\bar{A}_{0c}$, $\bar{A}_{1c}$, and $\bar{A}_{2c}$ couple the azimuth dynamics with the inclination dynamics, but this coupling is only present in terms of the inclination observer error and the integral action of the inclination observer. This fact is used advantageously, since the inclination observer error dynamics do not depend on the azimuth dynamics. Figure 6 depicts a cascaded structure showing how the tracking error dynamics and the observer error dynamics are interconnected.

Analyzing the inclination dynamics (top part of Figure 6), it is noted that these are independent from the azimuth dynamics and, furthermore, that the inclination observer error dynamics and inclination tracking error dynamics are in a series interconnection involving constant (ξ-independent) gain terms (see matrix $\bar{A}_{0\Theta}$ in (28)), which allows for the design of the inclination controller and observer gains separately based on the separation principle.

Second, the inclination observer error δ_Θ perturbs both the azimuth observer and tracking error dynamics (see Figure 6). δ_Θ is guaranteed to converge to zero exponentially if the poles of the (ξ-independent) inclination error dynamics are located in the open left-hand side of the complex plane (through the design of the L_Θ gain). The way δ_Θ is interconnected with the azimuth dynamics (see matrices $\bar{A}_{0c}$, $\bar{A}_{1c}$, and $\bar{A}_{2c}$ of (28)) is through ξ-dependent terms (namely, the "$p(\xi)$" terms in (28)). Nevertheless, these coefficients are only related to the designed reference trajectory, which means that they remain bounded according to the bounded reference trajectory. Considering the product of δ_Θ and the ξ-dependent input matrices of the azimuth observer error dynamics, this product is bounded and converges to zero exponentially. A similar remark holds for the way δ_Θ and δ_Φ perturb the azimuth tracking error dynamics.

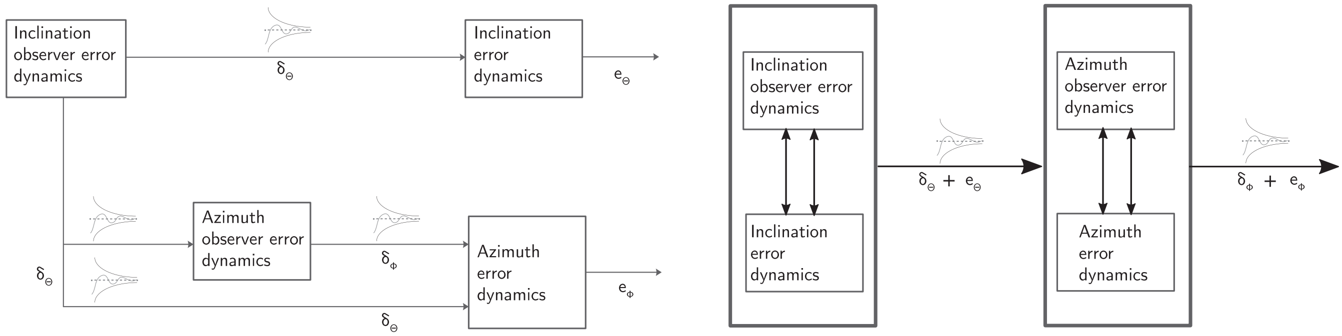

FIGURE 6 Cascaded structure of the linearized nominal (left) error dynamics in (27) and the linearized robust (right) error dynamics in (47)

Using this analysis of the cascaded decomposition of the error dynamics, the stability of the total (ξ-dependent) error dynamics can be guaranteed by the stability of the (ξ-*independent*) subsystems corresponding to the azimuth observer, and the tracking error dynamics (as in Figure 6) can be guaranteed without considering the perturbation terms (ie, using a cascaded systems argument).

Remark 5. An important observation is that the stability of the linearized system is independent from the actual desired trajectory, as this only influences the interconnection terms.

It can be concluded that the controller synthesis of gains K_i and L_i, for $i = \Theta, \Phi$, can be performed using a spectral approach for delay differential equations (see the work of Michiels and Niculescu[24]), for the following isolated partial error system dynamics (see Figure 6):

1. the isolated inclination and azimuth tracking error dynamics:

$$\begin{bmatrix} e'_\Theta(\xi) \\ \Delta\bar{\Gamma}^{*\prime}_\Theta(\xi) \\ \Delta z'_{1\Theta}(\xi) \\ \Delta z'_{2\Theta}(\xi) \end{bmatrix} = \begin{bmatrix} A_0 & 0 & 0 & B \\ 0 & -b_0 & 0 & -b_1 \\ \zeta_c \left[k_{1\Theta}, 0, 0 \right] & 0 & 0 & 0 \\ \gamma K_\Theta & 0 & \gamma & -\gamma \end{bmatrix} \begin{bmatrix} e_\Theta(\xi) \\ \Delta\bar{\Gamma}^*_\Theta(\xi) \\ \Delta z_{1\Theta}(\xi) \\ \Delta z_{2\Theta}(\xi) \end{bmatrix} + \begin{bmatrix} A_1 & 0 & 0 & 0 \\ 0 & 0 & 0 & 0 \\ 0 & 0 & 0 & 0 \\ 0 & 0 & 0 & 0 \end{bmatrix} \begin{bmatrix} e_\Theta(\xi_1) \\ \Delta\bar{\Gamma}^*_\Theta(\xi_1) \\ \Delta z_{1\Theta}(\xi_1) \\ \Delta z_{2\Theta}(\xi_1) \end{bmatrix} + \begin{bmatrix} A_2 & 0 & 0 & 0 \\ 0 & 0 & 0 & 0 \\ 0 & 0 & 0 & 0 \\ 0 & 0 & 0 & 0 \end{bmatrix} \begin{bmatrix} e_\Theta(\xi_2) \\ \Delta\bar{\Gamma}^*_\Theta(\xi_2) \\ \Delta z_{1\Theta}(\xi_2) \\ \Delta z_{2\Theta}(\xi_2) \end{bmatrix}, \tag{30}$$

$$\begin{bmatrix} e'_\Phi(\xi) \\ \Delta\Gamma^{*\prime}_\Phi(\xi) \\ z'_{1\Phi}(\xi) \\ z'_{2\Phi}(\xi) \end{bmatrix} = \begin{bmatrix} A_0 & 0 & 0 & B \\ 0 & -b_0 & 0 & -b_1 \\ \zeta_c \left[k_{1\Phi}, 0, 0 \right] & 0 & 0 & 0 \\ \gamma K_\Phi & 0 & \gamma & -\gamma \end{bmatrix} \begin{bmatrix} e_\Phi(\xi) \\ \Delta\Gamma^*_\Phi(\xi) \\ z_{1\Phi}(\xi) \\ z_{2\Phi}(\xi) \end{bmatrix} + \begin{bmatrix} A_1 & 0 & 0 & 0 \\ 0 & 0 & 0 & 0 \\ 0 & 0 & 0 & 0 \\ 0 & 0 & 0 & 0 \end{bmatrix} \begin{bmatrix} e_\Phi(\xi_1) \\ \Delta\Gamma^*_\Phi(\xi_1) \\ z_{1\Phi}(\xi_1) \\ z_{2\Phi}(\xi_1) \end{bmatrix} + \begin{bmatrix} A_2 & 0 & 0 & 0 \\ 0 & 0 & 0 & 0 \\ 0 & 0 & 0 & 0 \\ 0 & 0 & 0 & 0 \end{bmatrix} \begin{bmatrix} e_\Phi(\xi_2) \\ \Delta\Gamma^*_\Phi(\xi_2) \\ z_{1\Phi}(\xi_2) \\ z_{2\Phi}(\xi_2) \end{bmatrix}; \tag{31}$$

2. the isolated inclination and azimuth observer error dynamics:

$$\begin{bmatrix} \delta'_\Theta(\xi) \\ \Delta q'_\Theta(\xi) \end{bmatrix} = \begin{bmatrix} A_0 - L_\Theta C_\Theta & -B \\ \zeta_o \left[l_{1\Theta}, l_{2\Theta} \right] C_\Theta & 0 \end{bmatrix} \begin{bmatrix} \delta_\Theta(\xi) \\ \Delta q_\Theta(\xi) \end{bmatrix} + \begin{bmatrix} A_1 & 0 \\ 0 & 0 \end{bmatrix} \begin{bmatrix} \delta_\Theta(\xi_1) \\ \Delta q_\Theta(\xi_1) \end{bmatrix} + \begin{bmatrix} A_2 & 0 \\ 0 & 0 \end{bmatrix} \begin{bmatrix} \delta_\Theta(\xi_2) \\ \Delta q_\Theta(\xi_2) \end{bmatrix}, \tag{32}$$

$$\begin{bmatrix} \delta'_\Phi(\xi) \\ q'_\Phi(\xi) \end{bmatrix} = \begin{bmatrix} A_0 - L_\Phi C_\Phi & -B \\ \zeta_o \left[l_{1\Phi}, l_{2\Phi} \right] C_\Phi & 0 \end{bmatrix} \begin{bmatrix} \delta_\Phi(\xi) \\ q_\Phi(\xi) \end{bmatrix} + \begin{bmatrix} A_1 & 0 \\ 0 & 0 \end{bmatrix} \begin{bmatrix} \delta_\Phi(\xi_1) \\ q_\Phi(\xi_1) \end{bmatrix} + \begin{bmatrix} A_2 & 0 \\ 0 & 0 \end{bmatrix} \begin{bmatrix} \delta_\Phi(\xi_2) \\ q_\Phi(\xi_2) \end{bmatrix}. \tag{33}$$

Asymptotic stability can be achieved if gains K_i and L_i, for $i = \Theta, \Phi$, are designed in such a way that the poles of the delay differential equations (30), (31), (32), and (33) are in the open left-half of the complex plane. Moreover, the transient response of the isolated systems becomes faster if the poles are located further to the left in the complex plane. In order to synthesize the controller and observer gains, we formulate an optimization problem consisting in independently minimizing the spectral abscissa (see the work of Vanbiervliet et al[28]) described by the following objective functions:

$$J_1 = \max_{j \in [1,2,\dots,\infty]} \left\{ \Re \left(\lambda_{jK\Theta}(K_\Theta, \zeta_c, \gamma) \right) \right\}, \tag{34}$$

$$J_2 = \max_{j \in [1,2,\dots,\infty]} \left\{ \Re \left(\lambda_{jK\Phi}(K_\Phi, \zeta_c, \gamma) \right) \right\}, \tag{35}$$

$$J_3 = \max_{j \in [1,2,\dots,\infty]} \left\{ \Re \left(\lambda_{jL\Theta}(L_\Theta, \zeta_o) \right) \right\}, \tag{36}$$

$$J_4 = \max_{j \in [1,2,\dots,\infty]} \left\{ \Re \left(\lambda_{jL\Phi}(L_\Phi, \zeta_o) \right) \right\}, \tag{37}$$

where $\lambda_{jKi}(K_i, \zeta_c, \gamma)$ and $\lambda_{jLi}(L_i, \zeta_o)$, for $i = \Theta, \Phi$, represent the jth closed-loop pole of the isolated error systems corresponding to the controller and observer dynamics, respectively. These four objective functions correspond to each of the isolated systems (30), (31), (32), and (33). In general, these objective functions correspond to a nonsmooth, nonconvex optimization problem. The four independent nonsmooth optimization problems in (34)-(37) can be solved using a gradient sampling algorithm.[25] In order to reduce the computational effort in solving these optimization problems, the gains ζ_c and ζ_o of the integral action and the low-pass filter γ are fixed for each iteration. Note that the control objectives associated with γ, ζ_c, and ζ_o are on different "length" scales than those of the state-feedback and observer gains (see Remark 4) and can hence be designed separately. The values of the gains K_i and L_i are arbitrarily initialized.

Our purpose is not to find a global solution to the optimization problem but, rather, to obtain at least a solution that satisfies a particular stopping criterion. The stopping criterion for the optimization routine will be related to the location of the rightmost pole of each of the isolated error systems (30), (31), (32), and (33). In order to propose the values of these rightmost poles used in such stopping criterion, a desired length ("time") scale for the convergence of δ_i and e_i, for $i = [\Theta, \Phi]$, based on the cascaded structure of Figure 6 is introduced. The determining dynamics of the cascaded structure are given by the δ_Θ signal. Hence, it has been decided to set these dynamics as the *fast* (ie, short length scale) converging dynamics. As long as the other isolated dynamic systems have slower convergence, the inclination observer will not lead to large transients in the other dynamics (regarding δ_Φ, e_Θ, and e_Φ), which would potentially invalidate the assumptions motivating the stability analysis based on linearization. On the other hand, δ_Φ has to be faster than e_Φ; hence, it is placed in a *medium* length scale. For the error dynamics e_Θ and e_Φ, the choice can be made to set e_Θ in the same *medium* length scale as δ_Φ and to set e_Φ in a *long* length scale (since inclination does not depend on the azimuth). It has been decided to keep e_Θ and e_Φ on the same *long* length scale to have a similar tracking behavior for both Θ and Φ. The numerical values of the real part of the rightmost poles for these dynamics will be given in the simulation study of Section 6.

Remark 6. The optimization-based synthesis approach proposed in this paper cannot provide guarantees of the complex part of the closed-loop poles, and as such, a certain level of closed-loop transient oscillations cannot be avoided a priori. We note that approaches aiming to place the poles in a cone-wise section of the complex left-half plane, in an attempt to limit transient oscillations, are generally not feasible for the delay-type systems considered here.

5 | ROBUST STABILITY ANALYSIS AND CONTROLLER DESIGN

In directional drilling, there are two main parameters that can be considered to be both uncertain and highly influential in the system dynamics: the active weight on bit Π and the bit walk angle ϖ. The controller design of Section 4 was based on a nominal value of weight on bit Π. To test if the designed strategy is able to cope with the uncertainty of this parameter, it will be considered as $\Pi = \bar{\Pi} + \delta\Pi$, where $\bar{\Pi}$ represents the nominal value of weight on bit, Π is the actual weight on bit, and $\delta\Pi$ is the uncertainty on the weight on bit. The influence of ϖ will be analyzed by means of a simulation study in Section 6, since it introduces additional nonlinear coupling terms to the already complex dynamics of the system.

5.1 | Analysis of the closed-loop tracking error dynamics with uncertain Π

The stability of the system is assessed by first deriving the closed-loop error dynamics of the system considering uncertainty on the active weight on bit Π (ie, assuming no knowledge of the real active weight on bit), and stability is analyzed by means of linearization. This linearized version of the system dynamics is also used for the robust controller design in Section 5.2.

In this section, matrices $A_0, A_1, A_2, B_{0i}, B_{1i}, C_i$, and D_i, for $i = \Theta, \Phi$, are defined as in (6) and evaluated at $\Pi = \bar{\Pi} + \delta\Pi$. The versions of these matrices evaluated at the nominal active weight on bit $\bar{\Pi}$ are denoted by a bar symbol (ie, $\bar{A}_0$, $\bar{A}_1$, $\bar{A}_2$, $\bar{B}_{0i}$, $\bar{B}_{1i}$, $\bar{C}_i$, and $\bar{D}_i$). As before, the input filters are designed as follows:

$$\Gamma_i^{*\prime} = -\bar{b}_0\Gamma_i^* - \bar{b}_1 u_i, \tag{38}$$

where u_i is given by (14) and the coefficients $\bar{b}_0$ and $\bar{b}_1$ are defined as in (25) and evaluated at $\bar{\Pi}$. The feedforward is designed using the nominal versions of the system matrices as follows:

$$u_{ri} = B^T \left(x_{ri}'(\xi) - \bar{A}_0 x_{ri}(\xi) - \bar{A}_1 x_{ri}(\xi_1) - \bar{A}_2 x_{ri}(\xi_2) \right). \tag{39}$$

Also, the observer design is affected by the presence of uncertainty, which can be noted in the observer dynamics as follows:

$$\begin{aligned}\begin{bmatrix} \check{x}_\Theta' \\ q_\Theta' \\ \check{x}_\Phi' \\ q_\Phi' \end{bmatrix} &= \begin{bmatrix} \bar{A}_0 & 0 & 0 & 0 \\ 0 & 0 & 0 & 0 \\ 0 & 0 & \bar{A}_0 & 0 \\ 0 & 0 & 0 & 0 \end{bmatrix} \begin{bmatrix} \check{x}_\Theta(\xi) \\ q_\Theta(\xi) \\ \check{x}_\Phi(\xi) \\ q_\Phi(\xi) \end{bmatrix} + \begin{bmatrix} \bar{A}_1 & 0 & 0 & 0 \\ 0 & 0 & 0 & 0 \\ 0 & 0 & \bar{A}_1 & 0 \\ 0 & 0 & 0 & 0 \end{bmatrix} \begin{bmatrix} \check{x}_\Theta(\xi_1) \\ q_\Theta(\xi_1) \\ \check{x}_\Phi(\xi_1) \\ q_\Phi(\xi_1) \end{bmatrix} + \begin{bmatrix} \bar{A}_2 & 0 & 0 & 0 \\ 0 & 0 & 0 & 0 \\ 0 & 0 & \bar{A}_2 & 0 \\ 0 & 0 & 0 & 0 \end{bmatrix} \begin{bmatrix} \check{x}_\Theta(\xi_2) \\ q_\Theta(\xi_2) \\ \check{x}_\Phi(\xi_2) \\ q_\Phi(\xi_2) \end{bmatrix} \\ &+ \begin{bmatrix} L_\Theta(y_\Theta - \check{y}_\Theta) \\ \zeta[l_{1\Theta}, l_{2\Theta}](y_\Theta - \check{y}_\Theta) \\ L_\Phi(y_\Phi - \check{y}_\Phi) \\ \zeta[l_{1\Phi}, l_{2\Phi}](y_\Phi - \check{y}_\Phi) \end{bmatrix} + \begin{bmatrix} Bq_\Theta \\ 0 \\ Bq_\Phi \\ 0 \end{bmatrix} + \begin{bmatrix} B(u_{r\Theta} + v_\Theta) \\ 0 \\ B(u_{r\Phi} + v_\Phi) \\ 0 \end{bmatrix},\end{aligned} \tag{40}$$

with corresponding output equations

$$\check{y}_\Theta = \bar{C}_\Theta \check{x}_\Theta + \bar{D}_\Theta \Gamma^*_\Theta, \tag{41}$$

$$\check{y}_\Phi = \bar{C}_\Phi \check{x}_\Phi + \bar{D}_\Phi \Gamma^*_\Phi. \tag{42}$$

Since matrices C_i and D_i differ from their nominal versions ($\bar{C}_i$ and $\bar{D}_i$), the description for the derivatives of the states of the integral action for both inclination and azimuth is defined by (after substituting the output equations and considering the fact that $\check{x}_i = e_i + x_{ri} - \delta_i$)

$$q'_\Theta = \zeta[l_{1\Theta}, l_{2\Theta}] \left(\Delta C_\Theta e_\Theta + \Delta C_\Theta x_{r\Theta} + \Delta D_\Theta \Delta\Gamma^*_\Theta + \Delta D_\Theta \Gamma^*_{\Theta d} + \bar{C}_\Theta \delta_\Theta + EW_y\right), \tag{43}$$

$$q'_\Phi = \zeta[l_{1\Phi}, l_{2\Phi}] \left(\Delta C_\Phi e_\Phi + \Delta C_\Phi x_{r\Phi} + D_\Phi \left(\Delta\Gamma_\Phi + \Gamma^*_{\Phi d}\right)^* \frac{\sin\check{\Theta}}{\sin\Theta} - \bar{D}_\Phi \left(\Delta\Gamma^*_\Phi + \Gamma^*_{\Phi d}\right) + \bar{C}_\Phi \delta_\Phi\right), \tag{44}$$

where $\Delta D_i = D_i - \bar{D}_i$ and $\Delta C_i = C_i - \bar{C}_i$, for $i = \Theta, \Phi$. Using the above, the closed-loop error dynamics for state vector $X(\xi)$ (as defined in (23)) are obtained as follows:

$$\begin{aligned} X'(\xi) &= Q_{0\mathrm{cl}} X(\xi) + Q_{1\mathrm{cl}} X(\xi_1) + Q_{2\mathrm{cl}} X(\xi_2) \\ &\quad + U_{\mathrm{cl}} \left(u_{r\Theta}, u_{r\Phi}, \Gamma^*_{\Theta d}, \Gamma^*_{\Phi d}, x_{r\Theta}(\xi), x_{r\Theta}(\xi_1), x_{r\Theta}(\xi_2), x_{r\Phi}(\xi), x_{r\Phi}(\xi_1), x_{r\Phi}(\xi_2), \Theta, \check{\Theta}, W, W_y\right), \end{aligned} \tag{45}$$

where

$$Q_{0\mathrm{cl}} = \begin{bmatrix} Q_{0\Theta} & 0 \\ 0 & Q_{0\Phi}(\Theta, \Theta') \end{bmatrix}, \qquad Q_{1\mathrm{cl}} = \begin{bmatrix} Q_{1\Theta} & 0 \\ 0 & Q_{1\Phi} \end{bmatrix}, \qquad A_{2\mathrm{cl}} = \begin{bmatrix} Q_{2\Theta} & 0 \\ 0 & Q_{2\Phi} \end{bmatrix}, \tag{46}$$

and the system submatrices in (46) and the vector U_{cl} are given in Appendix B (for the complete derivation, see the work of Villarreal Magaña[22]).

Following the same approach as in the nominal case, the linearization of the system is performed at an equilibrium point. In doing so, additional difficulties are encountered due to the fact that for the robust case, $e_i \neq 0$ and $\delta_i \neq 0$ at equilibrium. The latter fact is caused by the fact that vector U_{cl} in (39) does not vanish for $e_i = \delta_i = 0$ due to the presence of parameter uncertainty (among other effects, this causes the feedforward to be inexact, which leads to nonconstant perturbations related to the ξ-dependent desired trajectory). Despite this fact, the same "equilibrium" point as in the nominal case is utilized, considering the fact that according to simulation results (see the work of Villarreal Magaña[22] and Assumption 3), even large variations in Π result in steady-state solutions close to the nominal equilibrium solution of the closed-loop system (see Appendix A).

Linearization is performed (in this case, using the actual value of Π) and defining the perturbation vector as in (27). The linearized system (considering that matrix $Q_{0\Phi}$ is ξ-dependent) is given by

$$\bar{X}'(\xi) = \bar{Q}_{0\mathrm{cl}} \bar{X}(\xi) + \bar{Q}_{1\mathrm{cl}} \bar{X}(\xi_1) + \bar{Q}_{2\mathrm{cl}} \bar{X}(\xi_2), \tag{47}$$

where the linearized system matrices $\bar{Q}_{0\mathrm{cl}}$, $\bar{Q}_{1\mathrm{cl}}$, and $\bar{Q}_{2\mathrm{cl}}$ are given by

$$\bar{Q}_{0\mathrm{cl}} = \begin{bmatrix} \bar{Q}_{0\Theta} & 0 \\ \bar{Q}_{0c} & \bar{Q}_{0\Phi} \end{bmatrix}, \qquad \bar{Q}_{1\mathrm{cl}} = \begin{bmatrix} \bar{Q}_{1\Theta} & 0 \\ \bar{Q}_{1c} & \bar{Q}_{1\Phi} \end{bmatrix}, \qquad \bar{Q}_{2\mathrm{cl}} = \begin{bmatrix} \bar{Q}_{2\Theta} & 0 \\ \bar{Q}_{2c} & \bar{Q}_{2\Phi} \end{bmatrix}. \tag{48}$$

Submatrices $\bar{Q}_{0i}$, $\bar{Q}_{1i}$, $\bar{Q}_{0i}$, $\bar{Q}_{0c}$, $\bar{Q}_{1c}$, and $\bar{Q}_{2c}$, for $i = \Theta, \Phi$, can be found in Appendix C.

The main difference with respect to the nominal case is that the separation principle between the controller and observer (for both the inclination and azimuth error dynamics) no longer holds, since there is mutual coupling between the tracking error dynamics and the observer error dynamics in both the inclination and azimuth error dynamics. This means that it is not possible to design controller and observer gains separately as in the nominal case. The latter also holds when pursuing a robust stability analysis given a controller designed for a nominal Π, which will also be performed in the benchmark study of Section 6.

Despite the fact that the separation principle no longer holds in the same way as in the nominal case, we recognize in (47) and (48) a ξ-dependent but unidirectional coupling from the inclination error dynamics to the azimuth error dynamics.

We remark that the perturbation terms in matrices $\bar{Q}_{0c}$, $\bar{Q}_{1c}$, and $\bar{Q}_{2c}$ in Equation (47) (see Appendix C) are bounded. As a consequence, the series connection between the inclination error dynamics and the azimuth error dynamics is asymptotically stable if the poles of the isolated closed-loop error systems formed by

$$X'_\Theta(\xi) = \bar{Q}_{0\Theta} X_\Theta(\xi) + \bar{Q}_{1\Theta} X_\Theta(\xi_1) + \bar{Q}_{2\Theta} X_\Theta(\xi) \tag{49}$$

$$X'_\Phi(\xi) = \bar{Q}_{0\Phi} X_\Phi(\xi) + \bar{Q}_{1\Phi} X_\Phi(\xi_1) + \bar{Q}_{2\Phi} X_\Phi(\xi) \tag{50}$$

are in the open left-half of the complex plane. In (49) and (50), the state vectors X_Θ and X_Φ correspond to the error states related to the inclination and azimuth, respectively, and matrices $\bar{Q}_{0i}$, $\bar{Q}_{1i}$, and $\bar{Q}_{2i}$ are defined as in Equation (48) and Appendix C.

5.2 | Robust controller design

On the basis of the analysis of the uncertain dynamics in Section 5.1, we pursue a robust controller design in this section. The values of ζ_c, ζ_o, and γ are designed to be the same as in the nominal case, following the same argument as in Section 4. The design of the gains K_i and L_i, for $i = \Theta, \Phi$, is based on the minimization of the two following objective functions:

$$J_{1r}(K_\Theta, L_\Theta) = \max_{j\in[1,2,\ldots,\infty]} \left\{ \Re\left(\lambda_{j\Theta}(K_\Theta, L_\Theta, \Pi)\right)\right\}, \tag{51}$$

$$J_{2r}(K_\Phi, L_\Phi) = \max_{j\in[1,2,\ldots,\infty]} \left\{ \Re(\lambda_{j\Phi}(K_\Phi, L_\Phi, \Pi))\right\}, \tag{52}$$

where λ_{ji}, for $i = \Theta, \Phi$, represents the closed-loop pole j of systems (49) and (50), respectively. Strictly speaking, in order to ensure robust stability against uncertainty of Π, the optimization based on the objective functions given by Equations (51) and (52) should be performed for all possible values of Π, which renders the optimization computationally unfeasible. An approach is adopted, where the objective function is minimized on a grid of values of Π given by $\Pi = \bar{\Pi} + \delta\Pi_i$, with $\delta\Pi_i$, ie,

$$\delta\Pi_i = -\delta\Pi_{\max} + \frac{i-1}{m-1} 2\delta\Pi_{\max}, \qquad \text{for } i \in \{1, 2, \ldots, m\}, \tag{53}$$

where m represents the number of grid points for which the closed-loop poles will be calculated. Note that m has to be chosen uneven and higher than 2 in order to include the nominal weight on bit $\bar{\Pi}$ into the objective function. Then, the minimization of the following objective functions (which correspond to (51) and (52) considering uncertain weight on bit) will be pursued:

$$\Psi(K_\Theta, L_\Theta) = \max_{i\in[1,2,\ldots,m]} \left(J_{1r}(K_\Theta, L_\Theta, \bar{\Pi} + \delta\Pi_i)\right), \tag{54}$$

$$\Psi(K_\Phi, L_\Phi) = \max_{i\in[1,2,\ldots,m]} \left(J_{2r}(K_\Phi, L_\Phi, \bar{\Pi} + \delta\Pi_i)\right). \tag{55}$$

Similarly as in the nominal case, the stopping criteria involving $\Psi(K_\Theta, L_\Theta)$ and $\Psi(K_\Phi, L_\Phi)$ are such that the resulting length scale of the inclination error dynamics is smaller than that of the azimuth error dynamics.

6 | SIMULATION RESULTS

We revisit the benchmark system as introduced in Section 3.1. The proposed trajectory is considered to represent a real desired borehole geometry and is a smooth, continuously differentiable trajectory in order to avoid sudden geometrical changes. The desired trajectory is given by an almost vertical section without curvature (hence a straight line), followed by a curved section and a straight horizontal section (see Figure 7).

6.1 | Nominal controller

Following the optimization-based synthesis approach discussed in Section 4 and using the nominal value of the active weight on bit Π, the values for the controller gains of the system are obtained and shown in Table C4.

Figure 8 shows the union of the closed-loop poles of the isolated systems (30), (31), (32), and (33) after implementing the controller gains in Table C4. The rightmost pole (poles at the origin are not considered since these are only introduced by the definition of the states involving average angles in the state-space dynamics; see also the work of Kremers[25]) is at −0.6195, which is indeed below the chosen maximum value for the rightmost poles of the error dynamics (see Table C4), guaranteeing asymptotic stability and providing transient performance. Figure 8 also expresses the desired “length scale” separation of the subsystem dynamics, as highlighted at the end of Section 4.

The tracking and observer errors are shown in Figure 9. The simulations are performed for several initial conditions using the nonlinear model given in (5) including the influence of gravity.

The error for both the inclination and the azimuth reaches steady state at approximately $\xi = 10$ (equivalent to 2.73 meters), and in the case of the observer error dynamics, steady state is reached at $\xi = 5$ (1.365 meters). These results comply with a fast enough response in order to drill a complex borehole geometry. It has to be mentioned that if the

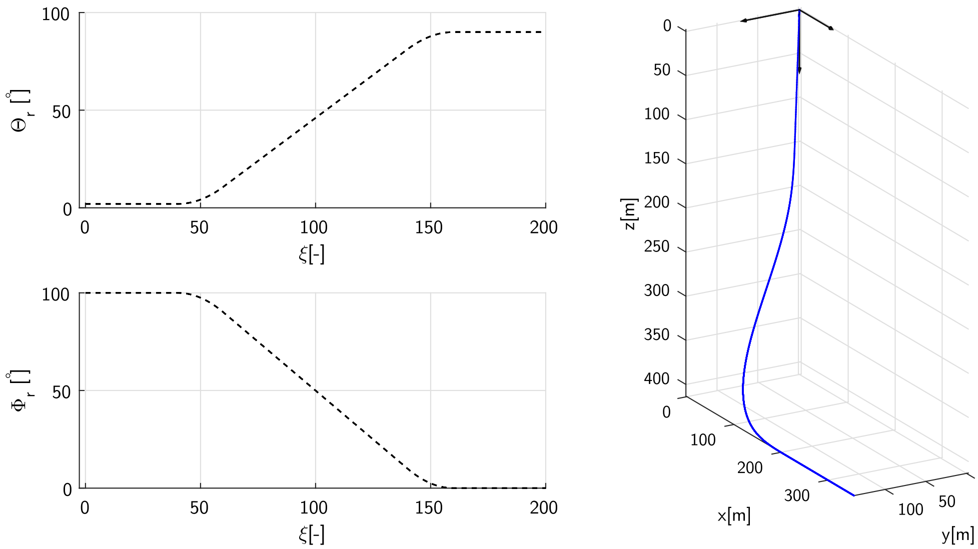

FIGURE 7 Desired borehole geometry and trajectory to be tracked [Colour figure can be viewed at wileyonlinelibrary.com]

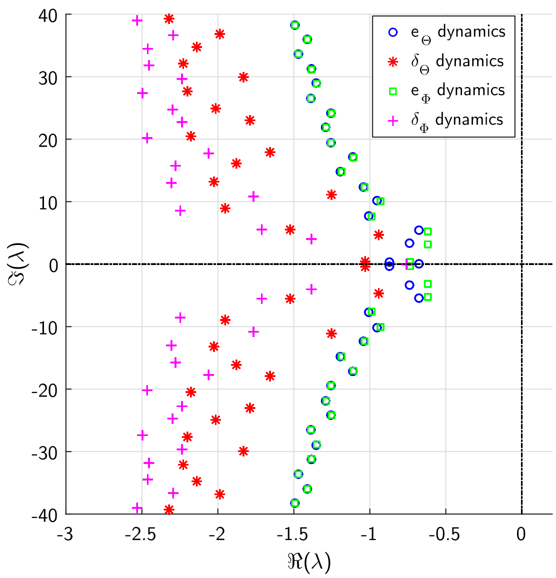

FIGURE 8 Closed-loop poles of the four different isolated error systems in (30), (31), (32), and (33) for the neutral bit walk system for $\Pi = 0.0087$ [Colour figure can be viewed at wileyonlinelibrary.com]

initial conditions are far away from the linearized error dynamics ($e_i = 0$ and $\delta_i = 0$, for $i = \Theta, \Phi$), the conditions under which the controller and observer were designed are no longer valid, and nonlinear terms may affect the transient performance of the system. In any case, it can be concluded that asymptotic tracking is achieved even for very large initial condition errors (see Figure 9). Finally, it can be noted that the control input shown in Figure 10 is dominated by the feedforward input after an initial transient, and the maximum values that Γ_Θ and Γ_Φ reach correspond approximately to 124.52 and 7.09 kN, respectively, in transients induced by the initial errors. We note that the RSS actuator forces, in practice, are typically limited within a range from 10 to 20 kN.[4] This means that the force applied by the input Γ_Θ exceeds the maximum achievable force in transients. However, in practice, the bit is initially positioned by experienced drillers (ie, close to the desired borehole trajectory), which means that the initial condition for the system will not be as far from the reference trajectory as displayed here in simulation (which was done for illustrative purposes). In the case of a set of initial conditions starting relatively close to the desired borehole trajectory ($\Theta_0 = 1°$, $\Phi_0 = 100°$; see Figure 10), the maximum RSS force is approximately 16.17 kN, which is feasible in practice.

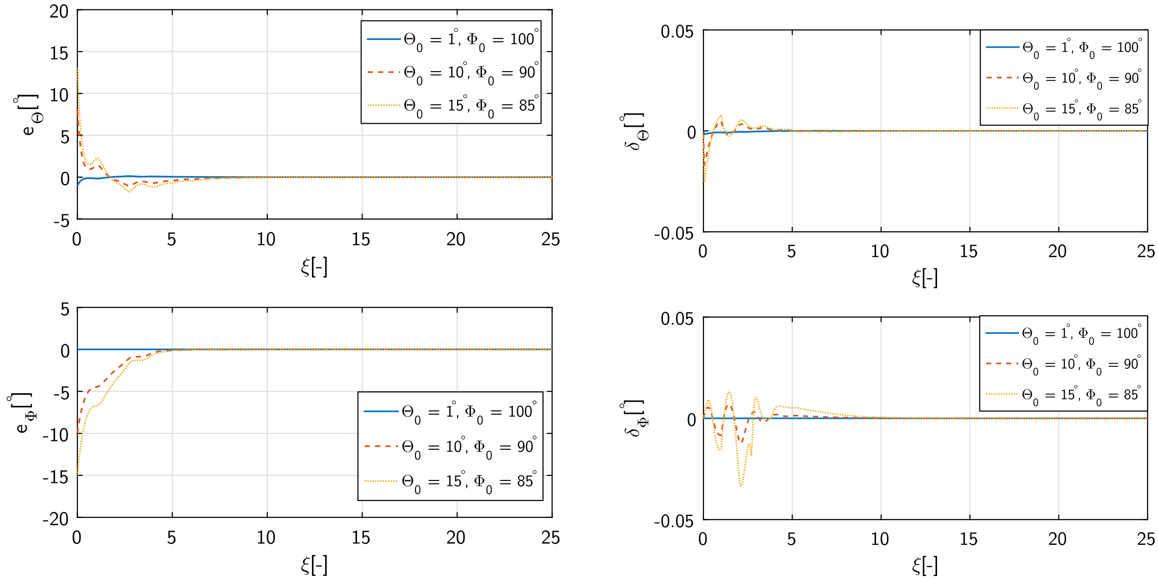

FIGURE 9 Tracking (left) and observer (right) error response for different initial conditions [Colour figure can be viewed at wileyonlinelibrary.com]

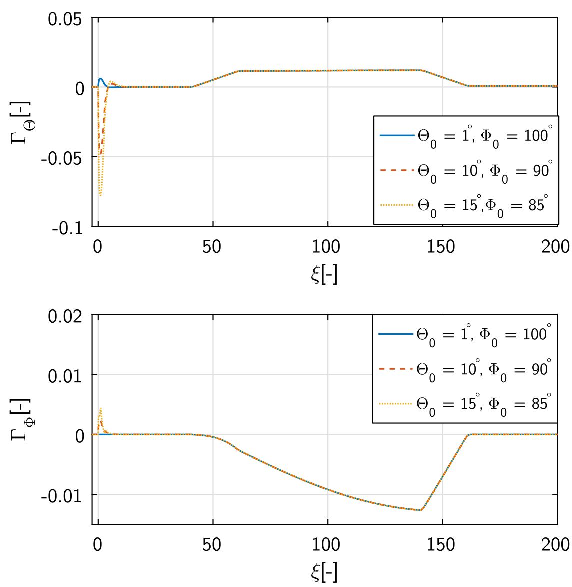

FIGURE 10 Control input applied to the system [Colour figure can be viewed at wileyonlinelibrary.com]

Robust stability of the nominal controller

The robust stability properties of the controller derived using the nominal active weight on bit are studied next. The robust stability analysis is performed by computing the rightmost pole of the closed-loop linearized total system dynamics given by Equation (47) and implementing the nominal controller designed above. These rightmost poles are computed for a variation of active weight on bit $\Pi \in [0.5\bar{\Pi}, 1.5\bar{\Pi}]$ for both the inclination and azimuth dynamics (see Figure 11). This Figure shows that the nominal controller has favorable robustness properties for a large uncertainty range. Nevertheless, Figure 11 shows that for smaller values of Π, stability may be compromised (reaching up to a real part of the rightmost pole of -0.02). This also has a detrimental effect on performance as it can be noted on the oscillatory behavior in Figure 12 with initial conditions $\Theta_0 = 15°$, $\Phi_0 = 85°$, for $\Pi = 0.0037(0.0043\bar{\Pi})$. In order to improve the robust stability and performance properties further, a robust controller design is pursued next.

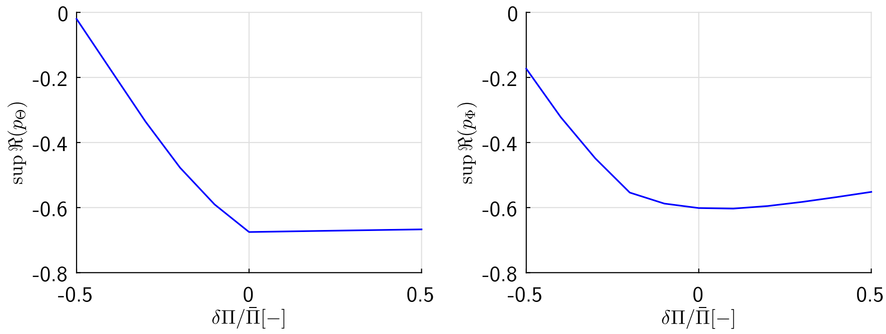

FIGURE 11 Robust stability test for inclination (left) and azimuth (right) error dynamics in (47) and (48) [Colour figure can be viewed at wileyonlinelibrary.com]

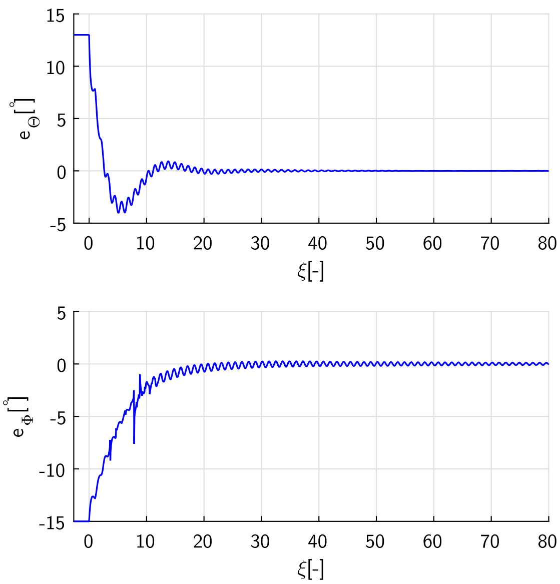

FIGURE 12 Error response for the nominal controller with $\Pi = 0.0037(0.43\bar{\Pi})$ [Colour figure can be viewed at wileyonlinelibrary.com]

6.2 | Robust controller design

The robust controller design strategy proposed in Section 5.2 is employed in this section. Considering that the integral action and low-pass filter gains are the same as in the nominal case (since they pursue objectives on a different length scale), Table C5 shows the gains of the controller and observer synthesized using the optimization-based approach for an uncertain value of Π for a grid of $m = 7$ according to Equation (53). Using this set of gains, the robustness of the controller is tested in the same way as in the nominal case. Figure 13 shows the location of the rightmost closed-loop pole with respect to the variation of Π for both the nominal and robust controller error dynamics. As shown in the Figure, there is a substantial improvement in the level of robustness in accordance with the design. Furthermore, it can be seen that the plots start to become "flat," ie, independent of Π (more evident in the case of the azimuth); this is considered a positive effect, since the rightmost pole is closer to the specified objective for every possible value of Π. This also has an effect on the performance of the system, eliminating the oscillations caused by the low value of the active weight on bit and reaching steady state at a shorter length (see Figure 14). It can be seen in Figure 15, as in the nominal case, that the control input is again dominated by the feedforward input, and furthermore, the magnitudes of the control inputs are also comparable to the ones in the nominal case, which means that the robust controller inputs are feasible in practice (the maximum force displayed for initial conditions $\Theta_0 = 1°$ and $\Phi_0 = 100°$ is again, approximately, 16.17 kN), despite the large difference in the observer and controller gains between the nominal (Table C4) and robust designs (Table C5).

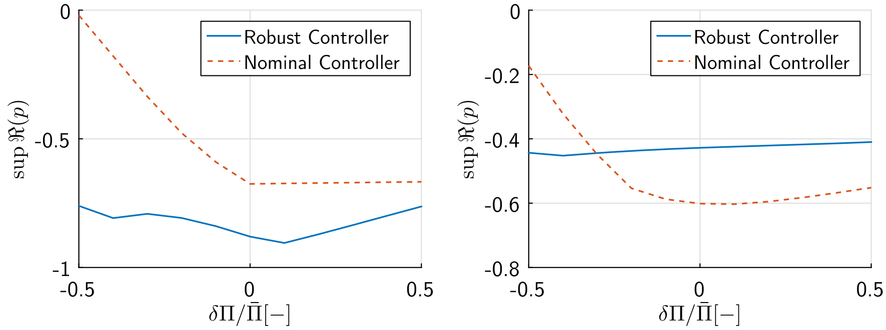

FIGURE 13 Robust stability comparison for inclination (left) and azimuth (right) error dynamics in (47) and (48) [Colour figure can be viewed at wileyonlinelibrary.com]

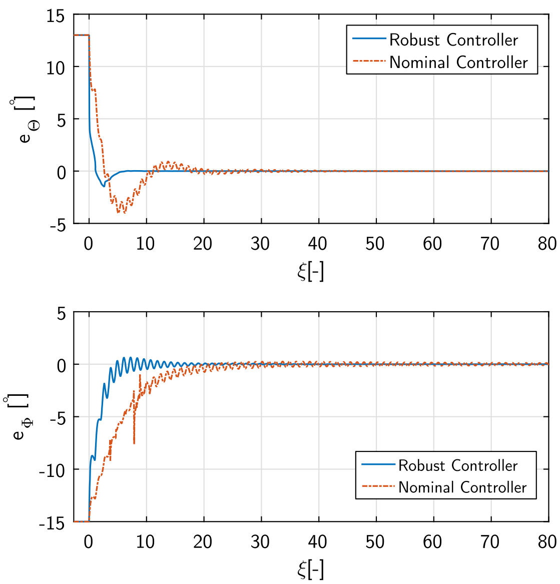

FIGURE 14 Comparison between the errors of nominal and robust controllers for $\Pi = 0.0037(0.43\bar{\Pi})$ [Colour figure can be viewed at wileyonlinelibrary.com]

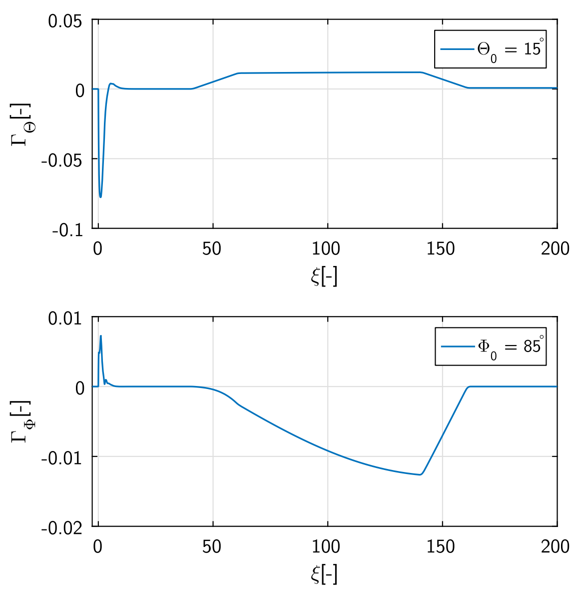

FIGURE 15 Control input applied on the system for $\Pi = 0.0037(0.43\bar{\Pi})$ and initial conditions $\Theta = 15°$, $\Phi = 85°$ [Colour figure can be viewed at wileyonlinelibrary.com]

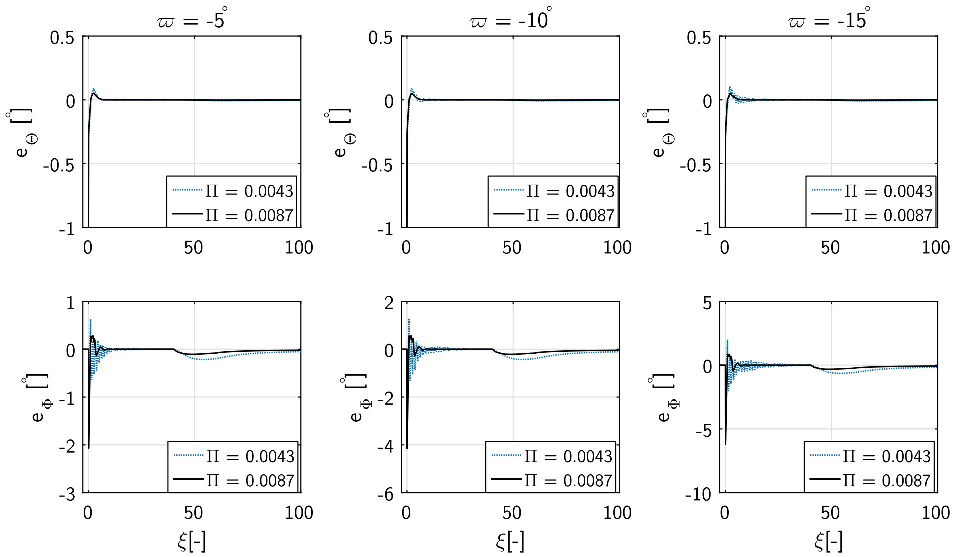

FIGURE 16 Simulation results of the neutral bit walk robust output-feedback controller for $\Pi = 0.5\bar{\Pi}$ (dotted line), $\Pi = \bar{\Pi}$ (solid line), $\Theta_0 = 1°$, $\Phi_0 = 100°$, and $\varpi \in \{-5°, -10°, -15°\}$ [Colour figure can be viewed at wileyonlinelibrary.com]

6.3 | Robust controller applied to non-neutral bit walk model

Finally, we apply the robust output-feedback controller that was designed for the neutral bit walk case to the case in which the bit walk is nonzero. We consider the model described by Equation (1) and $\varpi \neq 0$ in the output equations as well. We relax the initial conditions ($\Theta_0 = 1°, \Phi_0 = 100°$) with respect to the previous cases since the bit walk angle ϖ has a much more harmful effect in the system and the results would not be readable (due to an extremely high level of oscillations).

The simulation results are shown in Figure 16 for $\Pi = \bar{\Pi}$ and $\Pi = 0.5\bar{\Pi}$. These results show that the robust controller is still able to stabilize the system, which is not possible using the nominal controller design. However, the overall behavior shows transient oscillations (specially in the case of $\Pi = 0.5\bar{\Pi}$), which is not desired in practice. Hence, further research is needed on the controller design for directional drilling systems with a high bit walk angle.

7 | CONCLUSION

This paper proposes a robust output-feedback controller for a 3D drilling system. The control objective of being able to drill a complex borehole trajectory while avoiding borehole spiraling is expressed as a reference tracking problem. A controller was designed using the nonlinear delay system model developed in the work of Perneder[12] as a basis, considering the neutral bit walk condition. The key element of the proposed strategy is the inclusion of an observer in the control structure, which allows to rely only on the local measurements of the BHA orientation. In order to guarantee stability, a cascaded systems argument was used for the constructive synthesis of the controller and observer gains of the system. Moreover, a robust controller design was proposed, exhibiting robustness against significant uncertainties in the weight on bit and (moderate) uncertainty in the bit walk angle. The effectiveness of the proposed control strategy was evidenced via simulation studies.

ORCID

O.A. Villarreal Magaña http://orcid.org/0000-0002-2822-9216

REFERENCES

1. Downton GC, Klausen TS, Hendricks A, Pafitis D. New directions in rotary steerable drilling. *Oilfield Rev*. 2000;226(26):18-29.
2. Felczak E, Torre A, Godwin ND, et al. The best of both worlds—a hybrid rotary steerable system. *Oilfield Rev*. 2012;23(4):36-44.
3. Prensky S. Recent advances in well logging and formation evaluation. *World Oil*. 2010;231(6):51-57.

4. Marck J, Detournay E, Kuesters A, Wingate J. Analysis of spiraled borehole data using a novel directional drilling model. *SPE Drill Complet*. 2014;SPE-167992-MS:267-278. https://doi.org/10.2118/167992-MS
5. Matheus J, Ignova M, Hornblower P. A hybrid approach to closed-loop directional drilling control using rotary steerable systems. Paper presented at: SPE Latin America and Caribbean Petroleum Engineering Conference (LACPEC); 2014; Maracaibo, Venezuela.
6. Panchal N, Bayliss MT, Whidborne JF. Robust linear feedback control of attitude for directional drilling tools. Paper presented at: 13th IFAC Symposium on Automation in Mining, Mineral, and Metal Processing (IFAC MMM); 2010; Cape Town, South Africa.
7. Panchal N, Bayliss MT, Whidborne JF. Vector based kinematic closed-loop attitude control-system for directional drilling. Paper presented at: IFAC Workshop on Automatic Control in Offshore Oil and Gas Production; 2012; Trondheim, Norway.
8. Panchal N, Bayliss MT, Whidborne JF. Attitude control system for directional drilling bottom hole assemblies. *IET Control Theory Appl*. 2012;6(7):884-892. https://doi.org/10.1049/iet-cta.2011.0438
9. Bayliss M, Matheus J. Directional drilling tool simulation and system design. *SAE Int J Mater Manuf*. 2009;1(1):675-689. https://doi.org/10.4271/2008-01-1369
10. Neubert M, Heisig G. Mathematical description of the directional drilling process and simulation of directional control algorithm. *Zeitschrift fur Angewandte Math Mech (ZAMM)*. 1996;76:361-362.
11. Downton GC. Directional drilling system response and stability. Paper presented at: IEEE International Conference on Control Applications (CCA); 2007; Singapore, Singapore.
12. Perneder L. *A Three-Dimensional Mathematical Model of Directional Drilling* [thesis]. Minneapolis, MN: Faculty of the Graduate School, University of Minnesota; 2013.
13. Downton GC, Ignova M. Stability and response of closed loop directional drilling system using linear delay differential equations. Paper presented at: IEEE International Conference on Control Applications (CCA); 2011; Denver, CO.
14. Sun H, Li Z, Hovakimyan N, Ba T. $\mathscr{L}_1$ adaptive control for directional drilling systems. Paper presented at: IFAC Workshop on Automatic Control in Offshore Oil and Gas Production; 2012; Trondheim, Norway.
15. Kremers NAH, Detournay E, van de Wouw N. Model-based robust control of directional drilling systems. *IEEE Trans Control Syst Technol*. 2015;24(1):226-23. https://doi.org/10.1109/TCST.2015.2427255
16. van de Wouw N, Kremers NAH, Detournay E. Output-feedback inclination control of directional drilling systems. Paper presented at: 2nd IFAC Workshop on Automatic Control in Offshore Oil and Gas Production; 2015; Florianopolis, Brazil.
17. van de Wouw N, Monsieurs FHA, Detournay E. Dynamic state-feedback control of nonlinear three-dimensional directional drilling systems. Paper presented at: 10th IFAC Symposium on Nonlinear Control Systems (NOLCOS); 2016; Monterey, CA.
18. Perneder L, Detournay E. Anomalous behaviors of a propagating borehole. Paper presented at: SPE Deepwater Drilling and Completions Conference; 2012; Galveston, TX.
19. Perneder L, Detournay E. Equilibrium inclinations of straight boreholes. *SPE J*. 2013;18(3):395-405. https://doi.org/10.2118/160335-PA
20. Perneder L, Detournay E. Steady-state solutions of a propagating borehole. *Int J Solids Structures*. 2013;50(9):1226-1240. https://doi.org/10.1016/j.ijsolstr.2012.12.011
21. Monsieurs FHA. *Model-Based Decoupled Control of a 3D Directional Drilling System* [thesis]. North Brabant, Netherlands: Department of Mechanical Engineering, Eindhoven University of Technology; 2015.
22. Villarreal Magaña OA. *Robust Output-Feedback Control of 3D Directional Drilling Systems* [thesis]. Delft, Netherlands: Department of Mechanical, Maritime, and Materials Engineering, Delft University of Technology; 2016.
23. Chen S, Collins GJ, Thomas MB. Reexamination of PDC bit walk in directional and horizontal wells. Paper presented at: IADC/SPE Asia Pacific Drilling Technology Conference; 2008; Jakarta, Indonesia.
24. Michiels W, Niculescu SI. *Stability and Stabilization of Time-Delay Systems: An Eigenvalue-Based Approach*. Philadelphia, PA: SIAM; 2007. https://doi.org/10.1137/1.9780898718645
25. Kremers N. *Model-Based Robust Control of a Directional Drilling System* [thesis]. North Brabant, Netherlands: Department of Mechanical Engineering, Eindhoven University of Technology; 2013.
26. Detournay E, Richard T, Shepherd M. Drilling response of drag bits : theory and experiment. *Int J Rock Mech Mining Sci*. 2008;45(8):1347-1360. https://doi.org/10.1016/j.ijrmms.2008.01.010
27. Marck J, Detournay E. Influence of rotary-steerable-system design on borehole spiraling. *SPE J*. 2016;21(1):1-10. https://doi.org/10.2118/174554-PA
28. Vanbiervliet J, Verheyden K, Michiels W, Vandewalle S. A nonsmooth optimisation approach for the stabilisation of time-delay systems. *ESAIM: COCV*. 2008;14(3):478-493. https://doi.org/10.1051/cocv:2007060

How to cite this article: Villarreal Magaña OA, Monsieurs FHA, Detournay E, van de Wouw N. Robust output-feedback control of 3D directional drilling systems. *Int J Robust Nonlinear Control*. 2018;28:5915–5942. https://doi.org/10.1002/rnc.4362

APPENDIX A

p-COEFFICIENTS PRESENT IN CLOSED-LOOP LINEARIZED DYNAMICS IN THE NOMINAL CASE

In this appendix, the p-coefficients appearing in Equation (27) are given as follows:

$$p_{0e1}(\xi) = -B\frac{\mathcal{F}_r\Gamma^*_{\Phi d}}{\eta\Pi\sin\Theta_d}\begin{bmatrix} \beta_1\Theta_d + \beta_2\langle\Theta\rangle_{1d} + \beta_3\langle\Theta\rangle_{2d} + \beta_4\Theta_{1d} + \beta_5\Theta_{2d}\left(\frac{1}{\sin\Theta_d}\right) + \cdots \\ \left(-\beta_1 + \beta_2\langle\Theta\rangle_{1d} + \beta_3\langle\Theta\rangle_{2d} + \beta_4\Theta_{1d} + \beta_5\Theta_{2d}\right)\cos\Theta_d \\ -\beta_2\cos\Theta_d \\ -\beta_3\cos\Theta_d \end{bmatrix}^T - B\begin{bmatrix} \frac{\cos\Theta_d}{\sin\Theta_d}u_{r\Phi} \\ 0 \\ 0 \end{bmatrix}^T,$$

$$p_{0e2}(\xi) = -B\frac{\mathcal{F}_r\Gamma^*_{\Phi d}}{\eta\Pi\sin\Theta_d}\cos\Theta_d,$$

$$p_{0\delta 1}(\xi) = -B\frac{\mathcal{F}_r\Gamma^*_{\Phi d}}{\eta\Pi\sin\Theta_d}\begin{bmatrix} \beta_1\Theta_d + \beta_2\langle\Theta\rangle_{1d} + \beta_3\langle\Theta\rangle_{2d} + \beta_4\Theta_{1d} + \beta_5\Theta_{2d}\left(\frac{1}{\sin\Theta_d}\right) + \cdots \\ \left(-\beta_1 + \beta_2\langle\Theta\rangle_{1d} + \beta_3\langle\Theta\rangle_{2d} + \beta_4\Theta_{1d} + \beta_5\Theta_{2d}\right)\cos\Theta_d \\ -\beta_2\cos\Theta_d \\ -\beta_3\cos\Theta_d \end{bmatrix}^T$$
$$- B\begin{bmatrix} \frac{\cos\Theta_d}{\sin\Theta_d}u_{r\Phi} \\ 0 \\ 0 \end{bmatrix}^T + L_\Phi D_\Phi\begin{bmatrix} \Gamma^*_{\Phi d}\frac{\cos\Theta_d}{\sin\Theta_d} \\ 0 \\ 0 \end{bmatrix}^T,$$

$$p_{0\delta 2}(\xi) = -B\frac{\mathcal{F}_r\Gamma^*_{\Phi d}}{\eta\Pi\sin\Theta_d}\cos\Theta_d, \quad p_{0q}(\xi) = -\zeta\Gamma^*_{\Phi d}[l_{1\Phi}, l_{2\Phi}]D_\Phi\frac{\cos\Theta_d}{\sin\Theta_d},$$

$$p_{1e}(\xi) = B\frac{\mathcal{F}_r\Gamma^*_{\Phi d}\cos\Theta_d}{\eta\Pi\sin\Theta_d}[\beta_4\ 0\ 0], \quad p_{1\delta}(\xi) = B\frac{\mathcal{F}_r\Gamma^*_{\Phi d}\cos\Theta_d}{\eta\Pi\sin\Theta_d}[\beta_4\ 0\ 0],$$

$$p_{2e}(\xi) = B\frac{\mathcal{F}_r\Gamma^*_{\Phi d}\cos\Theta_d}{\eta\Pi\sin\Theta_d}[\beta_5\ 0\ 0], \quad p_{2\delta}(\xi) = B\frac{\mathcal{F}_r\Gamma^*_{\Phi d}\cos\Theta_d}{\eta\Pi\sin\Theta_d}[\beta_5\ 0\ 0],$$

where elements β_j, for $j \in \{1, 2, \ldots, 5\}$, correspond to the following elements of matrices A_0, A_1, and A_2:

$$\beta_1 = A_0(1,1), \quad \beta_2 = A_0(1,2), \quad \beta_3 = A_0(1,3), \quad \beta_4 = A_1(1,1), \quad \beta_5 = A_2(1,1). \tag{A1}$$

APPENDIX B

CLOSED-LOOP SYSTEM MATRICES WITH UNCERTAINTY ON Π

In this appendix, the full expressions for the closed-loop system submatrices with uncertainty on Π used in Section 5.1 are shown as follows:

$$Q_{0\Theta}=\left[\begin{array}{cccc|cc} A_0 & (B_{0\Theta}-B_{1\Theta}\bar{b}_0) & 0 & -B_{1\Theta}\bar{b}_1 & 0 & 0\\ 0 & -\bar{b}_0 & 0 & -\bar{b}_1 & 0 & 0\\ \zeta\left[k_{1\Theta},0,0\right] & 0 & 0 & 0 & -\zeta\left[k_{1\Theta},0,0\right] & 0\\ \gamma K_\Theta & 0 & \gamma & -\gamma & -\gamma K_\Theta & 0\\ \hline (\Delta A_0-L_\Theta\Delta C_\Theta) & (B_{0\Theta}-B_{1\Theta}\bar{b}_0-L_\Theta\Delta D_\Theta) & 0 & (-B-B_{1\Theta}\bar{b}_1) & \bar{A}_0-L_\Theta\bar{C}_\Theta & -B\\ \zeta\left[l_{1\Theta},l_{2\Theta}\right]\Delta C_\Theta & \zeta\left[l_{1\Theta},l_{2\Theta}\right]\Delta D_\Theta & 0 & 0 & \zeta\left[l_{1\Theta},l_{2\Theta}\right]\bar{C}_\Theta & 0 \end{array}\right],$$

$$Q_{0\Phi}=\left[\begin{array}{cccc|cc} A_0 & (B_{0\Phi}-B_{1\Phi}\bar{b}_0) & 0 & -B_{1\Phi}\bar{b}_1 & 0 & 0\\ 0 & -\bar{b}_0 & 0 & -\bar{b}_1 & 0 & 0\\ \zeta\left[k_{1\Phi},0,0\right] & 0 & 0 & 0 & -\zeta\left[k_{1\Phi},0,0\right] & 0\\ \gamma K_\Phi & 0 & \gamma & -\gamma & -\gamma K_\Phi & 0\\ \hline (\Delta A_0-L_\Phi\Delta C_\Phi) & \left(B_{0\Phi}-B_{1\Phi}\bar{b}_0-L_\Phi\left(D_\Phi\frac{\sin\check{\Theta}}{\sin\Theta}-\bar{D}_\Phi\right)\right) & 0 & (-B-B_{1\Phi}\bar{b}_1) & \bar{A}_0-L_\Phi\bar{C}_\Phi & -B\\ \zeta\left[l_{1\Phi},l_{2\Phi}\right]\Delta C_\Phi & \zeta\left[l_{1\Phi},l_{2\Phi}\right]\left(D_\Phi\frac{\sin\check{\Theta}}{\sin\Theta}-\bar{D}_\Phi\right) & 0 & 0 & \zeta\left[l_{1\Phi},l_{2\Phi}\right]\bar{C}_\Phi & 0 \end{array}\right],$$

$$Q_{ji}=\left[\begin{array}{cccc|cc} A_j & 0 & 0 & 0 & 0 & 0\\ 0 & 0 & 0 & 0 & 0 & 0\\ 0 & 0 & 0 & 0 & 0 & 0\\ 0 & 0 & 0 & 0 & 0 & 0\\ \hline \Delta A_j & 0 & 0 & 0 & \bar{A}_j & 0\\ 0 & 0 & 0 & 0 & 0 & 0 \end{array}\right],$$

$$P_{\mathrm{cl}}(\xi,\xi_1,\xi_2,\Theta,\check{\Theta},W,W_y)=\left[\begin{array}{c} F_{p\Theta}+(-B-B_{1\Theta}\bar{b}_1)u_{r\Theta}\\ 0\\ 0\\ 0\\ \hdashline F_{r\Theta}+(-B-B_{1\Theta}\bar{b}_1)u_{r\Theta}\\ \zeta\left[l_{1\Theta},l_{2\Theta}\right]\left(\Delta C_\Theta x_{r\Theta}+\Delta D_\Theta\Gamma^*_{\Theta d}+EW_y\right)\\ \hline F_{p\Phi}+(-B-B_{1\Phi}\bar{b}_1)u_{r\Phi}\\ 0\\ 0\\ 0\\ \hdashline F_{r\Phi}+(-B-B_{1\Phi}\bar{b}_1)u_{r\Phi}\\ \zeta\left[l_{1\Phi},l_{2\Phi}\right]\left(\Delta C_\Phi x_{r\Phi}+\left(D_\Phi\frac{\sin\check{\Theta}}{\sin\Theta}-\bar{D}_\Phi\right)\Gamma^*_{\Phi d}\right) \end{array}\right],$$

for $i=\Theta,\Phi$ and $j=1,2$. The expressions for F_{ri}, for $i=\Theta,\Phi$, are given by

$$F_{r\Theta}=(B_{0\Theta}-B_{1\Theta}\bar{b}_0-L_\Theta\Delta D_\Theta)\Gamma^*_{\Theta d}+(\Delta A_0-L_\Theta\Delta C_\Theta)x_{r\Theta}(\xi)+\Delta A_1x_{r\Theta}(\xi_1)+\Delta A_2x_{r\Theta}(\xi_2)+BW-L_\Theta EW_y, \tag{B1}$$

$$F_{r\Phi}=\left(B_{0\Phi}-B_{1\Phi}\bar{b}_0-L_\Phi\left(D_\Phi\frac{\sin\check{\Theta}}{\sin\Theta}-\bar{D}_\Phi\right)\right)\Gamma^*_{\Phi d}+(\Delta A_0-L_\Phi\Delta C_\Phi)x_{r\Phi}(\xi)+\Delta A_1x_{r\Phi}(\xi_1)+\Delta A_2x_{r\Phi}(\xi_2), \tag{B2}$$

where $\Delta A_0=A_0-\bar{A}_0$, $\Delta A_1=A_1-\bar{A}_1$, and $\Delta A_2=A_2-\bar{A}_2$.

APPENDIX C

CLOSED-LOOP LINEARIZED SYSTEM MATRICES WITH UNCERTAINTY ON Π

In this appendix, the full expressions of the closed-loop linearized system submatrices used for stability analysis in Section 5.1 are shown as follows:

$$
\bar{Q}_{0i} = \left[\begin{array}{cccc|cc}
A_0 & (B_{0i} - B_{1i}\bar{b}_0) & 0 & -B_{1i}\bar{b}_1 & 0 & 0 \\
0 & -\bar{b}_0 & 0 & -\bar{b}_1 & 0 & 0 \\
\zeta\left[k_{1i}, 0, 0\right] & 0 & 0 & 0 & -\zeta\left[k_{1i}, 0, 0\right] & 0 \\
\gamma K_i & 0 & \gamma & -\gamma & -\gamma K_i & 0 \\
\hline
(\Delta A_0 - L_i \Delta C_i) & (B_{0i} - B_{1i}\bar{b}_0 - L_i \Delta D_i) & 0 & (-B - B_{1i}\bar{b}_1) & A_0 - L_i \bar{C}_i & -B \\
\zeta\left[l_{1i}, l_{2i}\right]\Delta C_i & \zeta\left[l_{1i}, l_{2i}\right]\Delta D_i & 0 & 0 & \zeta\left[l_{1i}, l_{2i}\right]\bar{C}_i & 0
\end{array}\right],
$$

$$
\bar{Q}_{0c} = \left[\begin{array}{cccc|cc}
p_{0e1}(\xi) & p_{0e2}(\xi) & 0 & p_{0e3}(\xi) & p_{0e4}(\xi) & p_{0e4}(\xi) \\
0 & 0 & 0 & 0 & 0 & 0 \\
0 & 0 & 0 & 0 & 0 & 0 \\
0 & 0 & 0 & 0 & 0 & 0 \\
\hline
p_{0\delta 1}(\xi) & p_{0\delta 2}(\xi) & 0 & p_{0\delta 3}(\xi) & p_{0\delta 4}(\xi) & p_{0\delta 5}(\xi) \\
0 & 0 & 0 & 0 & p_{0q}(\xi) & 0
\end{array}\right],
$$

$$
\bar{Q}_{ji} = \left[\begin{array}{cccc|cc}
A_j & 0 & 0 & 0 & 0 & 0 \\
0 & 0 & 0 & 0 & 0 & 0 \\
0 & 0 & 0 & 0 & 0 & 0 \\
0 & 0 & 0 & 0 & 0 & 0 \\
\hline
\Delta A_j & 0 & 0 & 0 & A_j & 0 \\
0 & 0 & 0 & 0 & 0 & 0
\end{array}\right], \qquad
\bar{Q}_{jc} = \left[\begin{array}{cccc|cc}
p_{je1}(\xi) & 0 & 0 & 0 & p_{je2}(\xi) & 0 \\
0 & 0 & 0 & 0 & 0 & 0 \\
0 & 0 & 0 & 0 & 0 & 0 \\
0 & 0 & 0 & 0 & 0 & 0 \\
\hline
p_{j\delta 1}(\xi) & 0 & 0 & 0 & p_{j\delta 2}(\xi) & 0 \\
0 & 0 & 0 & 0 & 0 & 0
\end{array}\right],
$$

for $i = \Theta, \Phi$ and $j = 1, 2$. The definition of the p-coefficients inside the coupling matrices $\bar{Q}_{0c}$ and $\bar{Q}_{jc}$ will depend on the chosen linearization point.

TABLE C1 Geometric properties of the benchmark system

I_r [m]	O_r [m]	A [m^2]	I [m^4]	ℓ_1 [m]	ℓ_2 [m]	$\Lambda\ell_1$ [m]
0.0533	0.0857	0.0141	3.6×10^{-5}	3.66	6.10	0.61

TABLE C2 Material properties of the benchmark system

E_y [N/m^2]	ρ [kg/m^3]
2×10^{11}	7800

TABLE C3 Dimensionless parameters of the benchmark system

$\varkappa_1$	$\varkappa_2$	Λ	χ	η
1	1.67	0.167	0.1	30

TABLE C4 Controller and observer gains

Subsystem	Rightmost Pole Location	Feedback Controller Gains	γ	ζ_c, ζ_o
(30)	−0.6	$k_{1\Theta} = -6310, k_{2\Theta} = -2571, k_{3\Theta} = 1288$	0.8	0.5
(32)	−0.9	$l_{1\Theta} = 1014, l_{2\Theta} = 3299$	–	0.5
(31)	−0.6	$k_{1\Phi} = -2146, k_{2\Phi} = -1050, k_{3\Phi} = 524$	0.8	–
(33)	−0.7	$l_{1\Phi} = -48.5, l_{2\Phi} = 2555$	–	0.3

TABLE C5 Robust controller settings and gains

Dynamics	Objective Rightmost Pole	Controller Gains (K_i)	Observer Gains (L_i)
Inclination (Θ)	−0.7	$[-123987, 27068, 4104]$	$\begin{bmatrix} 121 & 3192 \\ 0 & 0 \\ 0 & 0 \end{bmatrix}$
Azimuth (Φ)	−0.4	$[-13595, 1071, 1202]$	$\begin{bmatrix} -1058 & 3243 \\ 0 & 0 \\ 0 & 0 \end{bmatrix}$